Electrochemical Society

101, No. [illegible] 195[illegible]

UNIV. OF MICHIGAN
[illegible]
EAST ENGINEERING
LIBRARY

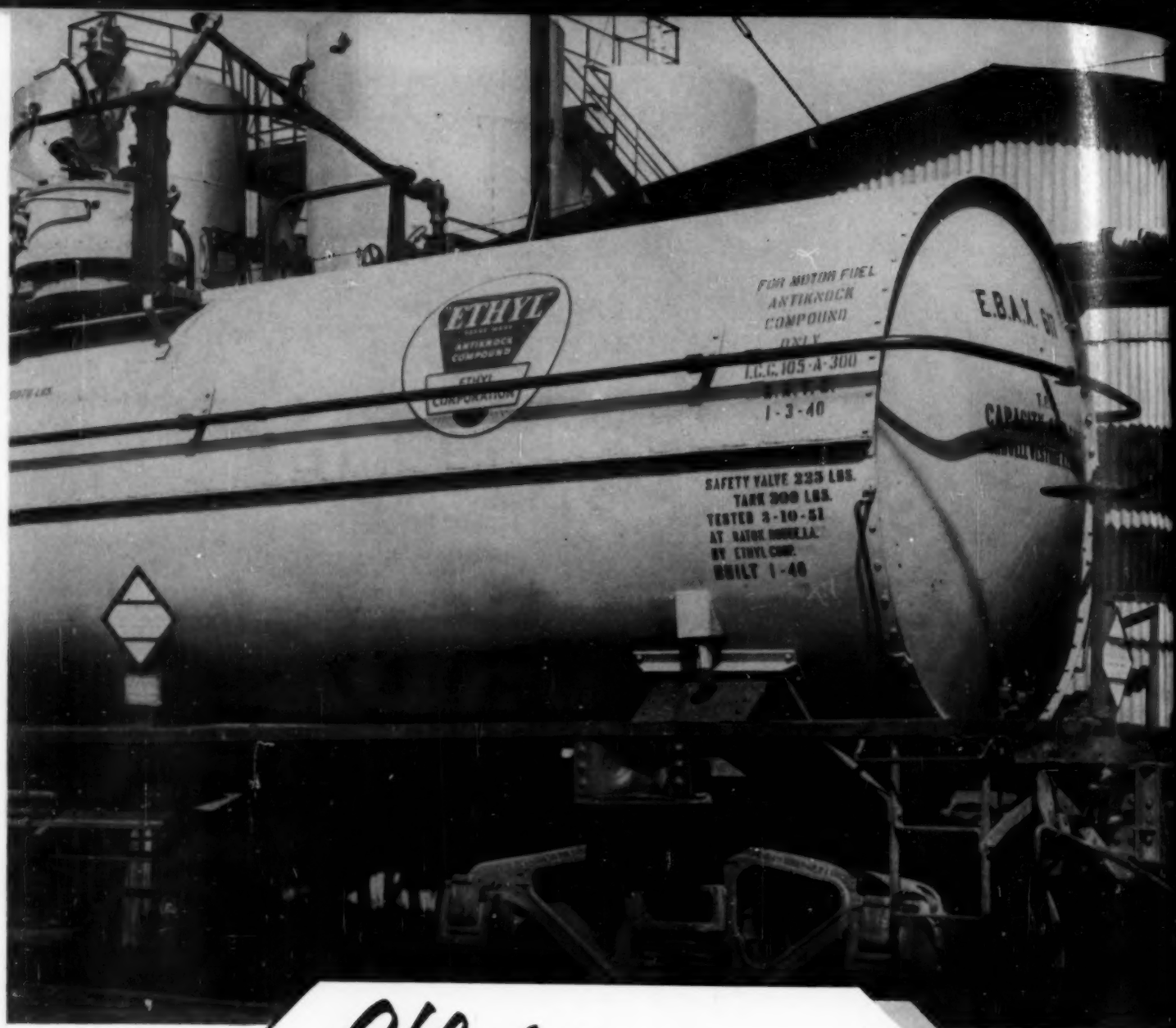

Courtesy Ethyl Corporation

Chlorine ...

for antiknock compounds

Ethyl chloride, ethylene dichloride and ethylene dibromide play an important part in the manufacture of antiknock compounds for combustion engine gasolines.

Uniformly high quality GLC Graphite Anodes play an important part too—in helping the electrolytic industry meet the growing civilian and defense needs for chlorine and caustic soda.

ELECTRODE DIVISION

Great Lakes Carbon Corporation

Niagara Falls, N.Y. GLC® Morganton, N. C.

Graphite Electrodes, Anodes, Molds and Specialties

Sales office: Niagara Falls, N.Y. **Other offices:** New York, N.Y., Oak Park, Ill., Pittsburgh, Pa.

Sales Agents: J. B. Hayes, Birmingham, Ala.; George O'Hara, Long Beach, Cal.; Great Northern Carbon & Chemical Co., Ltd., Montreal, Canada

Overseas Carbon & Coke Company, Inc., Geneva, Switzerland; Great Eastern Carbon & Chemical Co., Inc., Chiyoda-Ku, Tokyo

The Söderberg Self-Baking Electrode[1]

M. O. Sem

Elektrokemisk A/S, Oslo, Norway

ABSTRACT

The paper discusses the difference between electrode paste as used for prebaked electrodes and Söderberg electrodes. Baking conditions in a self-baking electrode are described. The quality depends on the calcining temperature of the dry material. New equipment giving improved baking conditions for the electrode is described.

Introduction

Consumption of Söderberg electrodes in the United States totals approximately 300,000 tons per year, while another 180,000 tons are consumed annually in Canada. Most of this is consumed in furnaces for the production of aluminum. Lately, however, a number of large carbide furnaces in the USA have been provided with Söderberg electrodes so that its use is now considerable in smelting furnaces. A discussion of conditions existing in the Söderberg electrodes is, therefore, of considerable interest.

Söderberg Electrode Paste

Carbon electrode paste is made of material like calcined anthracite—alone, or with petroleum coke or pitch coke mixed with a carbonaceous binder such as a medium pitch. Exact composition of the paste depends on the product of the electric furnace, i.e., in aluminum pots the paste must be made from petroleum coke or pitch coke in order not to introduce impurities into the produced metal. In most other cases, calcined anthracite is used predominantly. When first developed, the paste for Söderberg electrodes in Norway was made as closely as possible to the paste used for prebaked carbon electrodes. The latter are pressed from a rather dry paste in heavy hydraulic presses, or by other high pressure means. This could not easily be applied to the Söderberg electrode since it is made up in place over the furnace in which it is used. It was generally believed that it would not be possible to make in this way an electrode which would compete successfully with prebaked electrodes. During the first tests it became evident that conditions prevailing in the Söderberg electrodes during baking differ radically from those of prebaked electrodes. A much softer paste is required in order to attain satisfactory operation. The production of a self-baking electrode is an art which cannot be understood from the previous procedure.

Actually, it was found that Söderberg electrodes were highly improved in quality with increase in binder. The reason is that the baking zone in the electrode during its use is more or less horizontal, moving slowly upward as the electrode is lowered into the electric furnace to make up for electrode consumption. The soft paste in the upper part of the electrode rests with its weight on the baking zone and settles as the first volatiles are driven off during baking. Volatiles cannot rise in the electrode, but must escape downward through the pores of the already baked electrode and out the casing. This part of the electrode is incandescent (800°–900°C), and descending tar vapors passing through the carbon are cracked, leaving a considerable amount of carbon in the pores. This condition is illustrated in Fig. 1 and 2 which apply to a Söderberg electrode in a closed steel furnace and in an aluminum furnace, respectively.

Cracking of the volatiles can be studied easily in the laboratory by passing tar vapors slowly through a porous carbon electrode at temperatures between 600°–800°C. Results of such experiments (Table I) show a decided improvement in the quality of the electrode paste with higher carbon deposition. Thus, 2–3% carbon increases the crushing strength by more than 150 kg/cm^2.

Evidently, the quality of a Söderberg electrode depends on the amount of tar fumes forced through the porous part of the baked electrode. Actually, the content of binder in the electrode paste is made as high as practicable—under ordinary conditions, 4–10% more than in a paste used for prebaked electrodes. The actual content of binder in the paste depends on conditions and must be adjusted to the raw material of the electrode as well as to circumstances prevailing in the electrode while it is in use.

This condition may be illustrated by saying that there is no upper limit to the amount of binder that may be used in the Söderberg paste, but there

[1] Manuscript received March 12, 1954. This paper was prepared for delivery before the Chicago Meeting, May 2 to 6, 1954.

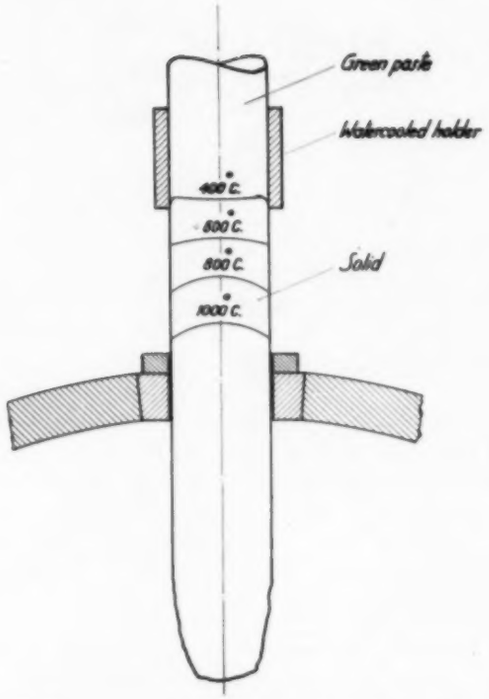

FIG. 1. Temperature zones in a Söderberg electrode in a teel furnace.

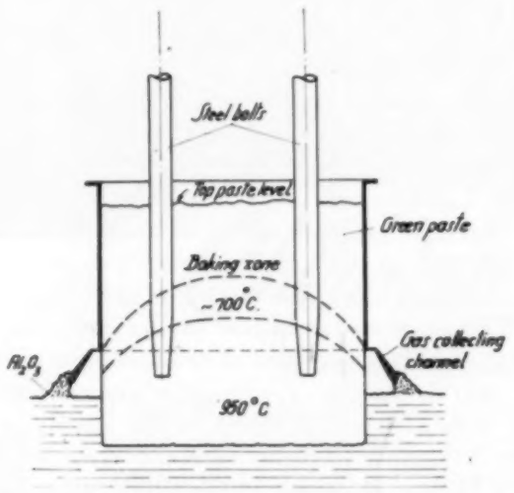

FIG. 2. Temperature zones and baking zone in a Söderberg aluminum anode.

is a decided lower limit, which is sufficiently high to render this paste useless in prebaked electrodes. Ordinarily, 18% binder is minimum.

ON CALCINING OF ANTHRACITE AND PETROLEUM COKE

These materials are calcined prior to use in the Söderberg electrode paste because volatile matter must be driven off, and shrinking of materials during calcination finished, before the binder is mixed in. If not, the electrode will crack during operation because volatiles of the binder are driven off at a lower temperature than the last fraction of volatiles contained in the dry materials. Shrinking takes place at temperatures where volatiles have been evaporated.

TABLE I

Temp, °C	Increase in weight	ohms/m/mm²	Apparent density	Crushing strength kg/cm²
No gas passed	—	128	1.38	203
700°C	1%	106	1.38	290
700°C	3.2%	94	1.42	363
800°C	2.3%	105	1.43	348

TABLE II

Anthracite		Electrode Paste		Baked Sample	
Type	El. resist. ohms/m/mm²	Binder content %	Loss in baking %	El. resist. ohms/m/mm²	Crushing strength kg/m/cm²
A	810	21	14.7	102	152
B	1280	19	12	104	254

For these reasons it is necessary to calcine raw materials at about 1200°C or more. The higher the calcining temperature, the more complete the shrinking and the higher the absolute density of the material. It has been found, however, that it is important not to calcine at a higher temperature than necessary. The higher the calcining temperature the more binder is needed for production of an electrode paste of a certain viscosity at operating temperatures. Many laboratory tests have been carried out showing that wetting the surface of the raw materials requires more binder, the higher the calcining temperature (Table II).

This table shows that an anthracite with higher resistance because of better wetting produces a much stronger electrode of approximately the same electrical conductivity.

These experiments show the importance of carrying out calcination under strictly controlled conditions. Actually, the best temperatures must be ascertained for each type of carbon material. Previously, calcining furnaces used for anthracite all over the world were electric shaft furnaces through which anthracite passed vertically. The material so produced has been found to be heterogeneous after calcination because electric current in the anthracite or coke concentrates in certain paths by virtue of the increase in conductivity with temperature. The calcined anthracite produced in these furnaces would therefore tend to be overheated along the center part of the furnace, while materials passing down the furnace walls would not be fully calcined. For petroleum coke, a gas- or oil-fired rotating kiln has been adopted to advantage. A higher temperature must be used for anthracite.

In order to calcine under fully controlled, even conditions an improved electric calcining furnace has been developed.[2] It is a rotating tube furnace, a part of which is provided with graphite electrodes. These are used to pass electric current through the anthracite, and temperature can be increased under strictly controlled conditions. Volatiles are burned and used to preheat the charge before it enters the heating zone at 600°–900°C. The power consumption of such a furnace is only 300–500 kwhr/metric ton of calcined anthracite. In comparison, the previous electric shaft furnace ordinarily consumed about 1000–1100 kwhr/metric ton. A furnace of about 50 tons of calcined anthracite per day is now operating in Norway.

Self-Baking of Electrodes

The quality of the baked Söderberg electrode, produced from a given electrode paste, is governed by the rate of baking and the efficiency of pyrogenic cracking of volatiles in pores of the electrode during the baking process. This is considered more fully in terms of conditions prevailing in a smelting furnace such as a carbide furnace.

Descent of the electrode into the smelting furnace depends on the electrode consumption, which again is dependent on the particular process carried out in the furnace. Ordinarily, dimensions of the electrode are determined by conditions existing in the furnace. It is therefore not possible to control electrode consumption in inches per day. Consumption, however, is practically even during operation of the furnace, which is continuous. The baking process progressing through the electrode during the operation is, however, not only governed by electrode consumption per day, but also to a large extent by slipping of the electrode through the water-cooled electrode holder. The baking conditions will be very different if the electrode is slipped through the holder frequently in short lengths or seldom, but farther each time. In ordinary smelting furnaces the baking zone in the electrode is found inside the water-cooled electrode holder in such a way that the electrode is ready baked in the lower part of the holder but unbaked in the upper part of it. Thus, the electrode takes the shape of the holder, and a good electrical contact is obtained. It is easy to determine the shape and place of the baking zone by introducing a long rod through the soft green paste in the upper part of the electrode.

Ordinarily, electrode consumption in furnaces for the production of carbide and ferrolloys, as well as in steel furnaces, amounts to approximately 4–20 in./day, according to conditions. Slipping electrodes weighing 15 tons or more through the holder has always been an awkward operation. The ordinary practice has been to slip the electrode at least 4–10 in. at a time. As seen from the baking zone, Fig. 1, every slip moves the baking zone downward in relation to the holder. After each slipping, the baking proceeds rapidly until the baking zone has again reached the starting position, where the cooling effect of the electrode holder reduces the baking rate strongly. After each electrode slip tar vapors in the baking zone are driven off very fast, and more violently the farther the electrode is slipped at each time. Since tar vapors must escape downward from the baking zone through the baked part of the electrode, such violent development of volatiles may easily result in accumulation of gas pressure in the electrode whenever the baking proceeds too fast.

At first it was the practice to make holes in the electrode casing in order to let tar vapors escape as easily as possible. This has disadvantages because the vapors condense on the electrode holder where they mix with dust and disturb the electrical contact. The most important drawback to this practice is that the tar vapor is not broken up sufficiently in the electrode pores. Thus, it has been found better to use a gas-tight electrode casing whereby the tar vapors must pass through a large part of the incandescent baked electrode. The baked electrode ordinarily has a porosity of 25% or more so that it is easy for gas to escape through this part of the electrode, provided it is developed rather evenly. If baking does not proceed slowly and evenly, gas pressure in the electrode may make it swell, and perhaps burst. (Fig. 3)

The paste swells between about 300°–400°C, depending markedly on rapidity of the temperature rise. Under ordinary conditions it does not affect the quality of the electrode. Best baking conditions are obtained if the electrode can slide continuously through the water-cooled electrode holder. For practical reasons this cannot be effected satisfactorily. It is necessary to let the electrode slide through the holder at intervals. However, baking of the electrode progresses more evenly, the shorter the slipping. Therefore, the equipment used for slipping should be remotely controlled by hydraulic, pneumatic, or similar means.

Electrode Holder

Details of the electrode equipment must vary for different furnaces according to conditions. One of the most difficult applications is to tilting furnaces. Söderberg electrodes have been adopted in such furnaces in some important installations in Norway, Sweden, Finland, France, and Italy. How-

[2] Through cooperation between Elektrokemisk A/S and F. L. Smidth & Co. A/S, Copenhagen.

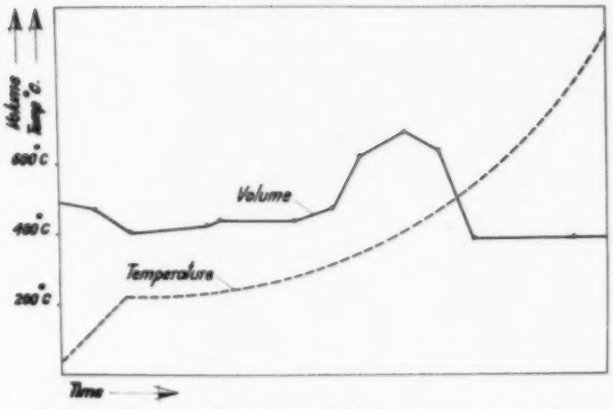

FIG. 3. Change of volume with the temperature during baking.

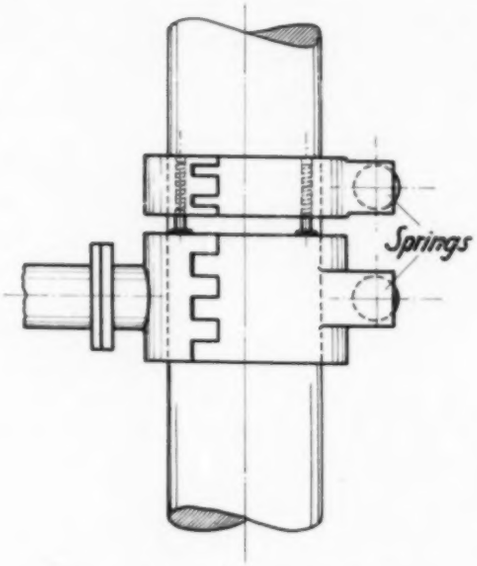

FIG. 4. Automatic slipping device

ever, conditions prevailing in these furnaces have presented particular difficulties for the following reasons:

1. Electrodes are ordinarily tilted with the furnace, which increases strain on the electrode.

2. Operation is batch type. There is little opportunity of resetting the electrode holder during heats.

3. Electrodes are ordinarily lengthened outside the furnace. Operation is therefore semicontinuous.

APPLICATION TO MELTING FURNACES

Electrode holders generally used in electric steel furnaces in Europe consist of 3 parts, one fixed and two gripped closely around the electrode like hinged jaws. The jaws are operated by means of a tangentially arranged screw. Ordinarily the holder is reset after each tapping during which the electrode is allowed to rest on the charge or on the furnace bottom. Conditions can be improved by operating the jaws by pneumatic or hydraulic pressure. However, it is difficult to use these means during operation and to control slipping as desired unless the electrode is allowed to rest on the charge or the furnace bottom.

In order to obtain good baking conditions in the electrode, a hydraulic or pneumatic device has been developed[3] which allows perfect control of slipping by simply turning a valve. The holder (1) is shown in Fig. 4. The hinged jaws have been maintained, but the tangential screw has been replaced by a spring-operated pressure device which clamps the jaws onto the electrode. The spring pressure may be released for slipping by applying compressed air or fluid pressure.

The slipping length is controlled by an automatically operated stopping device arranged on the electrode at the top of the holder. The stopping ring is like the holder except that ordinarily it has no current supply and is situated lower on the electrode. It is clamped around the electrode by fluid-operated springs exactly like those of the holder. It controls slipping by being clamped on to the electrode during the slipping. The electrode is stopped as soon as the ring hits the top of the holder. It is connected to and engages the holder with vertically arranged springs. These springs are compressed during slipping so that they automatically return the stopping ring to the initial distance above the holder as soon as the ring is released. During regular operation both holder and stopping ring clamp on to the electrode at the correct distance.

Ordinarily a slippage of 1–2 in. at a time is permitted. This insures a very smooth and safe movement under conditions which allow favorable baking of the electrode. The whole process is carried out by operating a couple of valves connected with the 3 electrode holders of the furnace.

Fig. 5 shows an electrode holder as installed in a 40-ton steel furnace of Christiania Spigerverk at Oslo. The holder has been tried out for more than 3½ years and has now been adopted for other furnaces in Norway and Sweden. It has contributed very much toward improving operating conditions in steel furnaces. In Scandinavia, where the choice is between graphite electrodes and Söderberg electrodes, consumption of the Söderberg type is somewhat less than twice that of graphite electrodes, while the cost of Söderberg electrodes is only about ⅓–¼ the cost of a graphite electrode. This applies to electrodes of 600–700 mm diameter. Actual electrode consumption in a 25-ton furnace of Christiania Spigerverk has been about 6–7 kg/metric ton of steel (cold charge).

[3] By Elektrokemisk A/S.

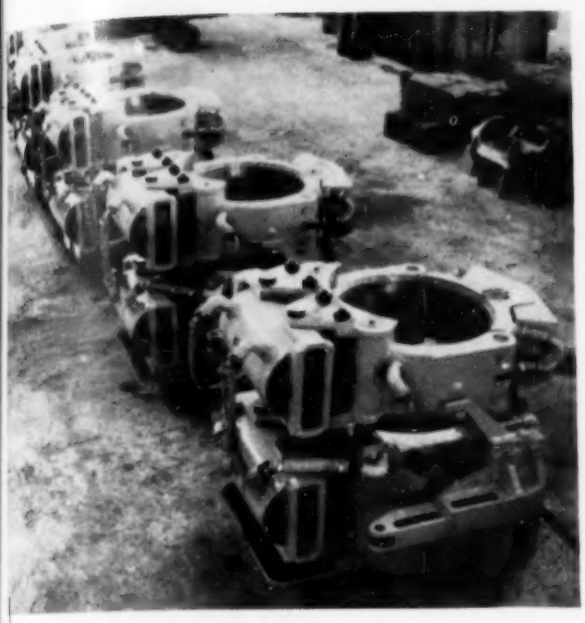

FIG. 5. Steel furnace electrode holder with automatic slipping device.

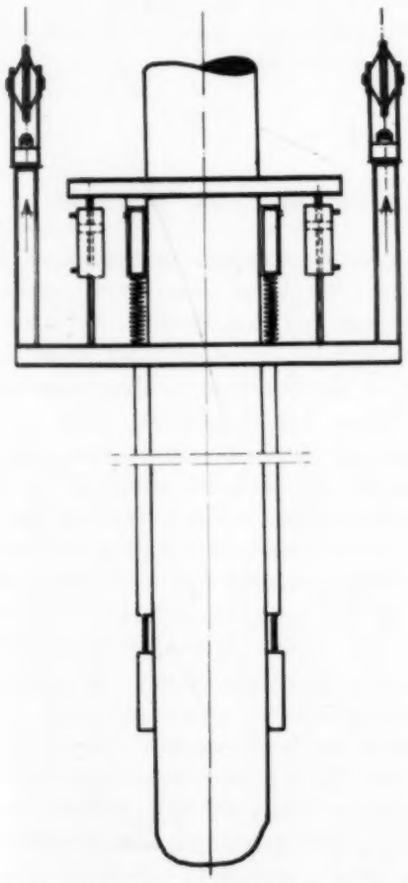

FIG. 6. Automatic slipping device for larger electrodes

APPLICATION TO SMELTING FURNACES

The slipping arrangement described above has also been successfully applied to Söderberg electrodes in furnaces for calcium carbide, ferro-alloys, and the like. Electrodes in such furnaces are ordinarily larger (up to 40–60 in. diameter). Details have been changed to meet the requirements of these big electrodes. Ordinarily, they are carried by an electrode holder which is suspended by a permanent iron casing surrounding the electrode for protection against dust and excessive heat (no baking is wanted above the electrode holder). This arrangement is shown in Fig. 6. The stopping ring is arranged at the top of the permanent iron casing and is designed for remote handling hydraulically. This makes possible a simple and perfectly controlled slipping process. Previously, slipping was controlled by applying Wisdom ribbons which were

FIG. 7. Electrode with mantle as Fig. 8

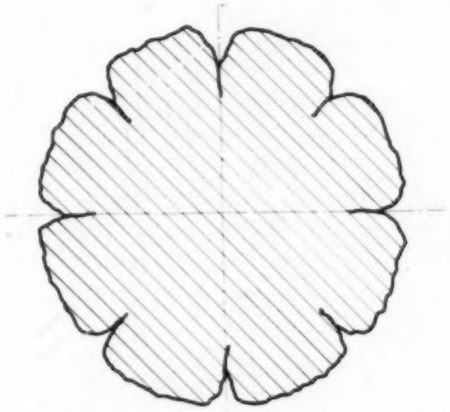

FIG. 8. Cross section of a baked Söderberg electrode under oxidizing conditions.

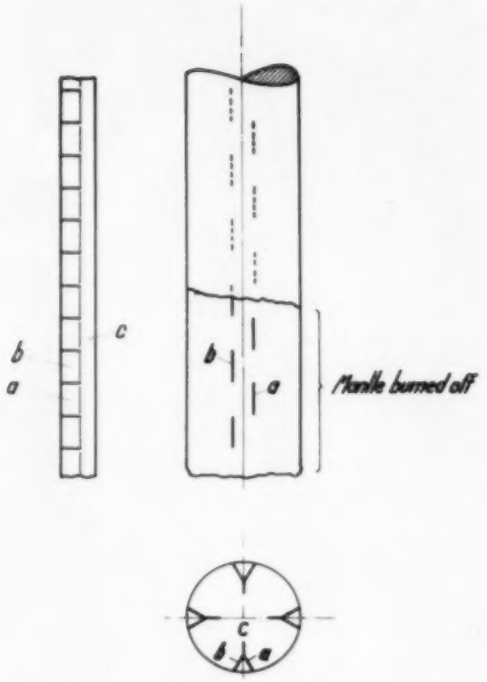

FIG. 9. New electrode mantle for steel furnace electrodes (Christiania Spigerverk).

welded to the electrode casing and consumed with the electrode.

The electrode holder has also been changed to hydraulic or pneumatic operation. This has greatly improved safety factors. At the same time, these electrode holders have been arranged inside a water-cooled, cylindrical casing which allows extension of the holder into the furnace through the furnace roof. Thereby the length of electrode from the lower end of the holder has been reduced, improving the electric conditions and simultaneously reducing strain to the electrode.

By slipping the electrode as described here, it has proved possible to simplify design of the iron casing with ribs which are filled with the electrode paste. The shape of the casing should be decided upon in each individual case. In melting furnaces a great deal of work has been done to improve the shape of the casing ribs also.

THE ELECTRODE CASING

The iron casing of the Söderberg electrode as described originally (2) is used in most furnaces all over the world. It insures good operation in most cases, but it has the drawback that the ribs form slots in the electrode periphery. This is a disadvantage if the furnace atmosphere is somewhat oxidizing, as in a steel furnace. In such a case, the lower part of the electrode may take on the shape shown in Fig. 7. Similar conditions are met in FeMn furnaces owing to O_2 development. This no

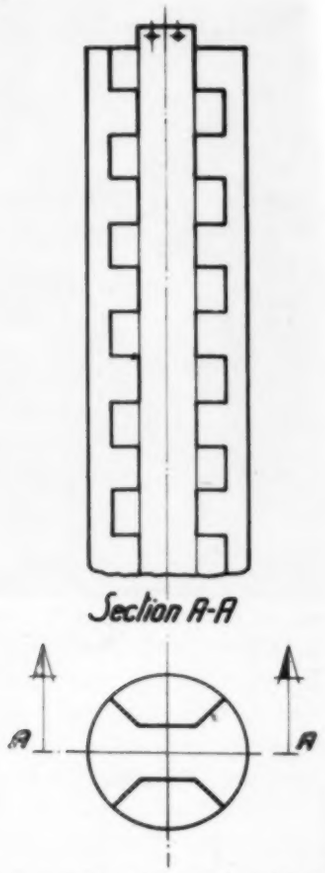

FIG. 10. Another method to avoid lengthwise slots in the baked electrode in steel furnaces (Sandviken).

doubt weakens the electrode and increases electrode consumption.

Fig. 8 shows an arrangement of ribs whereby continuous lengthwise slots have been avoided. Fig. 9 shows an electrode of this type in a steel furnace of Christiania Spigerverk.

A somewhat different arrangement has been developed by Sandvikens Jernverk in Sweden (Fig. 10). Even here the ribs form no slots in the periphery of the electrode, and they have been interconnected in such a way as to strengthen the electrode in the direction of tilting.

Both of these casing shapes are used in steel furnaces, but from operating results it has not yet been possible to decide which shape is better.

This paper has dealt mostly with electrodes in smelting and melting furnaces. Their use in aluminum furnaces is so different that it would require a separate paper. It has therefore been necessary to leave out this interesting application.

Any discussion of this paper will appear in a Discussion Section to be published in the June 1955 issue of the JOURNAL.

REFERENCES

1. K. FOYN, U. S. Pat. 2,668,183, April 2, 1923.
2. C. W. SÖDERBERG, U. S. Pat. 1,440,724, April 2, 1923.

Some Experiments with Scale Models of Electrothermic Furnaces[1]

OLUF CHR. BÖCKMAN

Elektrokemisk A/S, Oslo, Norway

ABSTRACT

Reproduction of temperature distribution in furnaces of different size is shown, by dimensional analysis, to require direct proportionality between power input and linear dimensions of the furnace, if transfer of heat by conduction is a controlling factor. Experiments with scale models indicate the importance of correct temperature gradients as a criterion of similarity. A 1:5 linear scale model of an industrial furnace for calcining anthracite has been successfully run according to this criterion. The principle has been extended to electric smelting furnaces with good results.

INTRODUCTION

Several authors (1–6) have compared the size of industrial electrothermic furnaces, especially the size of the electrodes, with the power input to the furnace at normal operation. Industrial furnaces are designed and operated to give the best operating and economic conditions, which conditions are incidentally carried into the comparison. The range of furnace sizes compared is relatively narrow, as the comparison naturally is limited to existing industrial furnaces.

In this paper, a different point of view is adopted. For research and development on electrothermic processes and furnaces, it is advantageous to perform experiments on small scale apparatus. The aim, therefore, is a drastic reduction of furnace size and a method of operating the furnace as a true model of an industrial furnace.

According to the established theory of models (7–9), physical and chemical processes taking place in the industrial furnace, the prototype, must be reproduced in the model. Usually it is not possible to reproduce all processes taking place in the prototype, if processes of inherently different nature are involved. This is certainly true in the case of many electrothermic furnaces. It is then necessary to evaluate the over-all importance of the different physical and chemical processes, in order to find the rate-determining or controlling factors.

Disregarding for the moment all other factors, it seems natural to concentrate attention on the evolution of heat. Obtaining high temperatures is essential to all electrothermic processes, which usually are sensitive to even small changes in the temperatures reached. Moreover, the temperature of an industrial furnace is not uniform within the reaction zone, but usually large temperature differences may be set up, which, in turn, impose definite conditions of the reaction zone. Thus it is necessary to reproduce not only the maximum temperature obtained in the prototype but, more significantly, the temperature distribution of the reaction zone.

Temperature differences are set up by the evolution and flow of heat. Evolution of heat may be controlled by the power input to the furnace. The flow of heat does not lend itself so readily to any control, except by deliberate design of the furnace and mode of operation.

In the reaction zone of an industrial furnace heat transfer by convection probably is insignificant. Radiant heat transfer may be important in some processes (2). It is felt, however, that heat transfer by conduction through the furnace charge and through the walls of the furnace is most important as far as temperature distribution of the reaction zone is concerned. It is assumed that reproduction of flow of heat by conduction is essential to the correct functioning of the model.

The correctness of this assumption may be tested for the simple case of a furnace where processes other than heat conduction are unimportant. Electric shaft furnaces for calcining anthracite are especially well adapted for this demonstration.

In more complex cases, e.g., electric smelting furnaces, other physical processes or even chemical reactions may to some extent become controlling factors. The over-all rate of the process may depend on diffusion of gases, e.g., diffusion of carbon monoxide for the reduction of metallic oxides. Diffusion in slag and/or metal may also be important, e.g., for reduction of metallic oxides in the slag by solid carbon, or reactions between slag and metal such as desulfurization of pig iron. Such diffusion processes usually are speeded up by any

[1] Manuscript received March 12, 1954. This paper was prepared for delivery before the Chicago Meeting, May 2 to 6, 1954.

turbulence set up by flow of the fluids, and so the pattern of gas flow or any stirring of liquid phases may be of importance. Even secondary physical processes may be important and, therefore, of a controlling nature. Thus, separation of metal and slag may be slow, or gas velocities may be high so as to nearly lift the burden. And any chemical reaction may become a controlling factor if the rate of the purely chemical reaction is low.

The importance of reproducing flow of heat by conduction even in these more complex cases may be demonstrated by the successful operation of models of smelting furnaces according to this criterion.

Dimensional Analysis

The total power to a furnace is dissipated in the following three ways: (*a*) heating the charge to reaction temperature; (*b*) supplying energy to match the heats of chemical reactions; and (*c*) heat losses. Or

$$P = q_1 + q_2 + q_3$$

where P = power input and the q's are heat terms.

The energy balance of a correct model must show the same distribution of the power input to the three heat absorbing items as is found in the prototype. Thus, the ratios q_1/P, q_2/P, and q_3/P must attain the same values in the model as in the prototype.

The parts of the power input q_1 required to heat up the charge, and q_2 to match the heats of chemical reactions are necessarily proportional to the rate of feed, w. Heat losses to the surroundings by conduction through the furnace charge and walls must set up in the model the same temperature differences in the reaction zone as are found in the prototype. This implies that temperature gradients in the model are larger than those in the prototype by the ratio of linear dimensions of prototype to model, since the same temperature difference shall be set up in the correspondingly shorter distance. By Fourier's equation for the conduction of heat,

$$q_{3/A} = k\frac{dT}{dD} \sim 1/D$$

the flow of heat per unit area is directly proportional to temperature gradient. D is taken as a representative linear dimension, e.g., the diameter of the furnace pot. If thermal conductivity, k, of furnace charge and walls are equal for corresponding points in model and prototype, the flow of heat per unit area is inversely proportional to linear dimensions of the furnace. The total heat losses by conduction dissipated from the surface of the furnace are then found by multiplying with area, or

$$q_3 \sim A/D \sim D$$

The model law then becomes

$$P \sim w \sim q_3 \sim D$$

The same results are obtained by a formal dimensional analysis of the problem, which shows that the dimensionless groups wc/kD (Graetz), hD/k (Nusselt), and a special dimensionless group P/kDT must attain the same values in the model as in the prototype. Here, c is the specific heat and h is the heat transfer coefficient. From the constancy of these groups is directly read

$$w \sim D$$

$$h \sim q_3/A \sim 1/D$$

$$P \sim D$$

If Ohm's law is applicable, and if electric resistivity of the furnace charge is equal for model and prototype, the ohmic furnace voltage will be equal for the two furnaces. This is seen from the constancy of the dimensionless group $P\rho/DE^2$, with E = ohmic furnace voltage and ρ electric resistivity. If the power input to the model is not made strictly proportional to the linear dimensions, or if electric resistivity of model furnace charge differs from that of the prototype, the furnace voltage will be given by

$$E^2 \sim P\rho/D$$

Discussion of Model Laws

The following consequences may be deduced from these model-to-prototype relationships:

1. The linear velocity of any stream of materials is inversely proportional to linear dimensions of the furnace.

2. The time necessary for a particle to pass through the furnace is proportional to the square of linear dimensions of the furnace.

3. The electric current density (e.g., in the electrodes) is inversely proportional to the linear dimensions of the furnace.

If all extensive properties (mass, quantity of heat, electricity, etc.) are considered proportional to the cube of linear dimensions, the three points may be stated collectively by saying that the time scale is proportional to the square of linear dimensions. By heating or cooling of solids, temperature distribution is known to be a function of the Fourier number, $k\theta/\rho_c D^2$, which clearly points out this relationship between time and linear scales. θ is time, and ρ is density.

If no other process than heat conduction is rate-determining, operating conditions of the prototype will be completely reproduced in the model by this

arrangement. If all parts of the system are reduced to scale, viz., lump size of the furnace charge reduced to scale, any diffusion process in the prototype will be reproduced in the model, which is seen from the formal correspondence between thermal and material diffusion. In addition, if gas velocities are low, the pattern of gas flow will be reproduced in the model, because the modified Reynolds number, based on particle size, will attain the same value in prototype and model.

Two factors of practical importance may, however, upset this simple relationship between prototype and model, viz., rapid flow of gases and slow chemical reactions or changes of physical structure within the reaction zone.

In a 1:5 linear scale model, the velocity of any gas stream is five times the velocity of the corresponding gas stream in the prototype. The ratio of velocity pressures is correspondingly 25:1. If the velocity pressure of gas flow is important in the prototype, the model will not function correctly in this respect when the operation of the model is based on the criterion of equal temperature distribution. This is the case when appreciable amounts of gases are evolved by the process. In the model, the velocity pressure of gas streams may then become exceedingly large, to the effect of lifting the burden of the furnace. It is impossible to reproduce correctly in the model both temperature distribution and velocity pressure, and a compromise must be made between the two conflicting demands.

The reduced time scale of the model requires, for the correct functioning of the model, that any chemical reaction or change of physical structure that takes place in the prototype shall occur in the model in a correspondingly shorter time. This is possible only if chemical reactions or changes of structure are sufficiently rapid to be no rate-determining step, even on the shorter time scale of the model. Fortunately, this requirement seems to be met in many cases, but in other cases the reactions obviously are too slow, and a compromise must be made between the conflicting demands.

Practical Applications

The theory has been applied to the operation of models of electric shaft furnaces for calcining anthracite and to models of electric smelting furnaces for the production of pig iron.

Fig. 1 shows the principle of the furnace for calcining anthracite. Raw anthracite is fed to the top of the furnace; on descending it is heated to calcining temperature by passage of electric current between top and bottom electrodes, and finally discharged at the bottom.

In calcining anthracite only small volumes of gases are evolved, and the velocity pressure of gas flow is unimportant even in the model. By calcination, the anthracite is changed from an electrically nonconductive material to a conducting substance by the expulsion of volatiles and change of physical structure, reactions which are very rapid. If the theory developed is sound, it should be possible to reproduce the process correctly in a model.

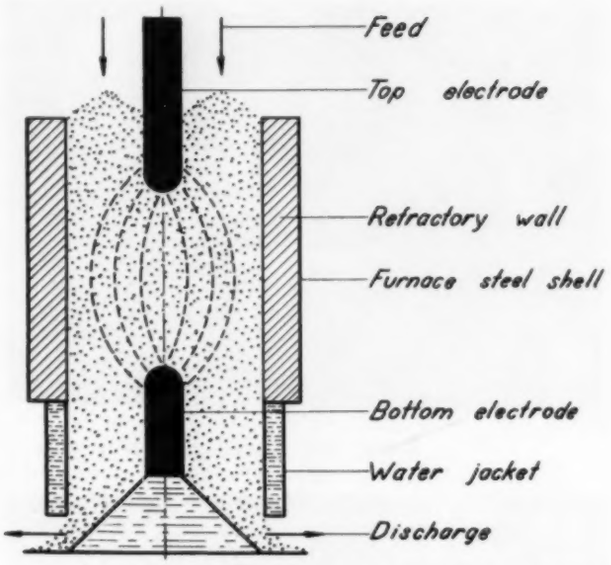

FIG. 1. Principle of the furnace for calcining anthracite

TABLE I. *Operation of a 1:5 linear scale model of calcining furnace*

	Prototype	Model
Power input, kw	735	112
Rate of feed, kg/h	640	94.3
Furnace voltage, v	54	50
Energy consumption, kwhr/kg	1.15	1.19
Temperature of discharge, °C	380	325
Electrical resistivity of product Ω mm²/m	450	500

A 1:5 linear scale model of a 750 kw industrial furnace was built and operated according to the theory. The correct flow of heat through the furnace lining was obtained by water-jacket cooling of the furnace steel shell.

Table I shows the corresponding figures for prototype and model. The voltage used for the operation of the model was slightly less than required by theory, because the transformer used could not give the correct voltage. Correspondingly the power input is somewhat less than required by theory. If the formula $E^2 \sim P\rho/D$ is used, observations check with theory on the assumption of 13% higher resistivity of model charge. The smaller burden weight in the model may reasonably count for this effect.

Measurements of temperature distribution of

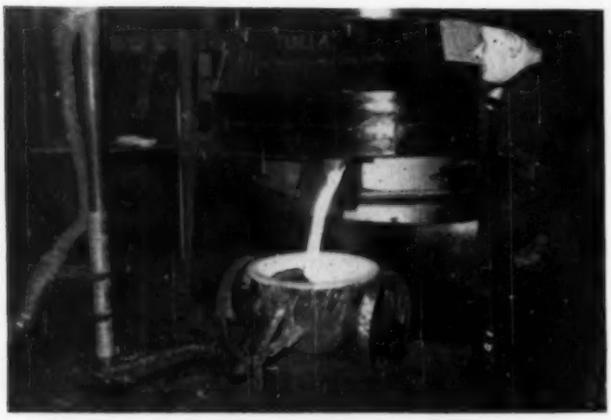

FIG. 2. 500-kw model

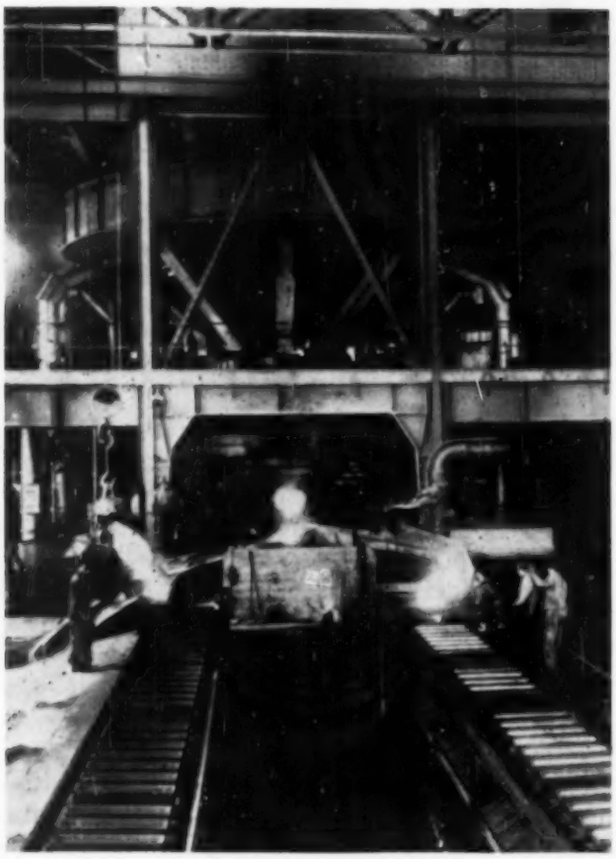

FIG. 3. 6000-kw prototype

prototype and model check well, and the quality of the product is well reproduced as indicated by the measurements of electrical resistivity.

The operation of a 1:4 linear scale model of one electrode of a three-phase 7500 kva pig iron furnace was undertaken to test the theory for the case of a smelting process. Table II shows that observations check reasonably well with theory even in this more complicated system. Operation of the furnace was somewhat difficult, obviously caused by the increased velocity of the gas flow. Metallurgical conditions of the prototype were, however, well reproduced, as indicated by the analyses of slag and metal produced. Reproduction of specific energy consumption is of special interest, because energy consumption of a process usually is of primary importance. Operation of this model on a variety of raw materials has shown remarkable correspondence to the operation of industrial furnaces on the same types of raw materials.

TABLE II. *Operation of a 1:4 linear scale model of one electrode of a three-phase 7500 kva pig iron furnace*

	Prototype	Model
Power input, kw	6000	500
Ohmic voltage, electrode to hearth, v	65	60
Energy consumption, kwhr/kg	2.5	2.51
% FeO in slag	1–2	2–4
% C in pig	3–4	3–4
% Si in pig	1–2	1–2

The conclusion is that it is possible to simulate operating conditions of industrial smelting furnaces by use of scale models.

Any discussion of this paper will appear in a Discussion Section to be published in the June 1955 issue of the JOURNAL.

REFERENCES

1. F. V. ANDREAE, *Trans. Electrochem. Soc.*, **63,** 309 (1933).
2. P. DROSSBACH, *Z. Elektrochem.*, **46,** 643 (1940).
3. G. VOLKERT AND E. SCHWARTZ VON BERGKAMPT, *Stahl u. Eisen*, **70,** 369 (1950).
4. R. DURRER AND G. VOLKERT, (Editors), "Die Metallurgie der Ferrolegierungen," pp. 46–49; E. SCHWARTZ VON BERGKAMPT, "Modellbetrachtung des Lichtbogenofens," Springer-Verlag, Berlin (1953).
5. R. B. PEACOCK, *Chemistry & Industry*, **1952,** 888.
6. H. A. CURTIS, *This Journal*, **100,** 81C (1953).
7. P. W. BRIDGMAN, "Dimensional Analysis," Yale University Press, New Haven (1943).
8. H. L. LANGHAAR, "Dimensional Analysis and Theory of Models," John Wiley & Sons, Inc., New York (1951).
9. M. W. THRING, *Trans. Inst. Chem. Eng., (London)*, p. 8, Oct. 26 (1948).

The pH in Chlorine-Caustic Electrolysis by the Mercury Cell Process[1]

LARS BARR

Division of Applied Electrochemistry, Royal Institute of Technology, Stockholm, Sweden

ABSTRACT

Anolyte composition in mercury cells for chlorine-caustic electrolysis is calculated as a function of *p*H, and the relation between anodic current loss and the anolyte *p*H is derived. Reactions between anodic and cathodic by-products and dependence of the cathodic current loss upon the anolyte *p*H are also discussed. Finally, certain components of the feed brine which affect *p*H of the anolyte are examined. It is demonstrated that optimum current efficiency with respect to both chlorine and caustic cannot be reached if *p*H of the anolyte is greater than 3, that stirring the cathode film, e.g., by solid particles on the mercury surface, decreases current efficiency, and that alkalinity of the feed brine, which must not exceed a certain value, is made up of the following concentrations:

$$[OH^-] + 2[CO_3^=] + [HCO_3^-] + [ClO^-].$$

INTRODUCTION

Several investigations have been carried out on the influence of various process variables on current efficiency in chlorine-caustic electrolysis by both the mercury and diaphragm cell processes. Thus, in a number of laboratory experiments, Taussig (1) estimated cathodic current efficiency in the mercury cell process as a function of amalgam concentration, current density, temperature, and salt concentration, i.e., brine flow. Johnson (2) measured anodic current loss as a function of current density, temperature, and salt concentration.

However, no investigation seems to have been published concerning the influence of *p*H of the electrolyte.

The mercury process is run in various ways, owing to brine purification methods, material problems, etc., with good results; consequently the question of *p*H may seem to be of minor importance, and the allowed *p*H range comparatively wide.

The purpose of the following calculations is to demonstrate more exactly the *p*H range suitable for the mercury cell process.

ELECTROLYTE EQUILIBRIUM COMPOSITION

Besides Na^+Cl^-, H_2O, and its ions, the following substances may occur in brine because of chlorine dissolution and anodic reactions: Cl_2, Cl_3^-, HClO, ClO^-, and ClO_3^- (3–5). In practice, the anode material is graphite; therefore, the system $CO_2 - H_2O$ is also present. Activities of these particular substances in equilibrium will now be calculated as functions of hydrogen ion activity $\{H_3O^+\}$, at 25° and 60°C and total pressure of 1 atm.

The chlorine system is defined by the following equations, in which braces, {}, denote the activity in mole/l and "(aq)" means that the substance is dissolved in water:

$$\frac{\{H_3O^+\}\{Cl^-\}\{HClO\}}{\{Cl_2(aq)\}} = K_1'\{H_2O\}^2 \simeq K_1 \qquad [1]$$

and

$$\frac{\{H_3O^+\}^6\{Cl^-\}^5\{ClO_3^-\}}{\{Cl_2(aq)\}^3} = K_2'\{H_2O\}^9 \simeq K_2 \qquad [2]$$

both involving electron exchange, and

$$\frac{\{H_3O^+\}\{ClO^-\}}{\{HClO\}} = K_s'\{H_2O\} \simeq K_s \qquad [3]$$

involving proton exchange.

The carbonic acid system is defined by the following equations, both involving proton exchange:

$$\frac{\{H_3O^+\}\{HCO_3^-\}}{\{H_2CO_3\}} = K_{s1}'\{H_2O\} \simeq K_{s1} \qquad [4]$$

and

$$\frac{\{H_3O^+\}\{CO_3^=\}}{\{HCO_3^-\}} = K_{s2}'\{H_2O\} \simeq K_{s2} \qquad [5]$$

If the water activity is assumed to be constant, which is an approximation, the right hand sides of equations [1–5] will be constant.

From investigations of Jakowkin (3) and Sand (4, 6), equilibrium constants of the chlorine system can be calculated. Jakowkin investigated the

[1] Manuscript received August 31, 1953. This paper was prepared for delivery before the Chicago Meeting, May 2 to 6, 1954.

HClO equilibrium, equation [1], at various temperatures between 13.4° and 57.5°C, while Sand studied the chlorate equilibrium, equation [2], at 20° and 70°C, and the protolysis of HClO, equation [3], at 17° and 70°C.

If concentrations of the diluted systems studied are assumed to be identical with activities, the following values are obtained: pK_1 (25°C) = 3.35; pK_2 (25°C) = 11.24; pK_s (25°C) = 7.36; pK_1 (60°C) = 3.02; pK_2 (60°C) = 11.04; pK_s (60°C) = 7.09; where $p = -\log$.

MacInnes and Belcher (7, 8) estimated the values of K_{s1} and K_{s2} at 25° and 38°C, which give: pK_{s1} (25°C) = 6.34; pK_{s2} (25°C) = 10.25; pK_{s1} (60°C) = 6.26; pK_{s2} (60°C) = 10.12.

The following equation was used for interpolation or extrapolation which had to be carried out to 25° and 60°C.

$$\frac{d \ln K}{dT} = \frac{\Delta H^0}{RT^2} \qquad [6]$$

in which T = absolute temperature, R = the gas constant, and ΔH^0 = standard enthalpy change. The latter was considered constant within the interval concerned.

As a general condition, it is now assumed that Cl_2(aq) and H_2CO_3 activities are constant at constant chlorine and carbon dioxide pressures, respectively, and at constant temperature. Since in this case activity is defined with reference to an infinitely dilute solution, it cannot be considered equal to the partial pressure of the gas, but only proportional to this pressure.

Provided the gas phase is ideal, the following equation concerning the chlorine system is obtained:

$$\{Cl_2(aq)\} = K_{1,Cl2} \cdot \mathfrak{p}_{Cl2} \qquad [7]$$

in which $\mathfrak{p}$ is the pressure in atmospheres and K_1 the thermodynamic solubility constant in mole/l atm. $K_{1,Cl2}$ was calculated by Whitney and Vivian (9) in the temperature range 10°–25°C, the activity coefficients being assumed equal to unity.

At 25°C the value of the constant $pK_{1,Cl2}$ (25°C) is 1.21. If their figures at 20°–25°C are extrapolated to 60°C with $pK_{1,Cl2}$ as a linear function of $1/T$, the value $pK_{1,Cl2}$ = 1.92 is obtained. Since such a long extrapolation is comparatively unreliable, the 60°C figure has also been calculated from an old investigation by Gay-Lussac (10), who measured the solubility of chlorine in water at various temperatures between 0° and 100°C. After correction for the HClO formation according to equation [1] and with the activity coefficients equal to unity, the figure $pK_{1,Cl2}$ (60°C) = 1.82 is obtained, which value is used here.

In the same way, the CO_2 system is defined by the equation:

$$\{H_2CO_3\} = K_{1,CO_2} \cdot \mathfrak{p}_{CO_2} \qquad [8]$$

pK_{1,CO_2} was calculated from the absorption coefficient of CO_2 in water at 25° and 60°C (11). After correction for HCO_3^- formation according to equation [4] and with activity coefficients equal to unity, the following values were obtained: pK_{1,CO_2} (25°C) = 1.47 and pK_{1,CO_2} (60°C) = 1.80.

A mercury cell is generally operated in the concentration range, 250–310 g/l NaCl, so the equilibrium calculation will be carried out for both 250 and 310 g/l NaCl.

If activity coefficients of the univalent ions are assumed to be 0.9 (12) at both salt concentrations and both temperatures, which is an approximation due to rapid alteration of the coefficients in this concentration range, the following chloride ion activities are obtained: $p\{Cl^-\}$(250 g/l) = −0.58; $p\{Cl^-\}$(310 g/l) = −0.68. Approximate mean value = −0.6.

The gas phase composition is characterized by:

$$\mathfrak{p}_{Cl_2} + \mathfrak{p}_{CO_2} + \mathfrak{p}_{H_2} + \mathfrak{p}_{H_2O} = 1 \text{ atm} \qquad [9]$$

in which $\mathfrak{p}_{H_2O}$ = 0.025 atm at 25°C and 0.16 at 60°C (13).

If the dried chlorine gas contains, for example, 1.0% CO_2 and 0.5% H_2, $\mathfrak{p}_{Cl_2}$ (25°C) = 0.96 atm, $\mathfrak{p}_{Cl_2}$ (60°C) = 0.83 atm, $\mathfrak{p}_{CO_2}$ (25°C) = 0.010 atm, and $\mathfrak{p}_{CO_2}$ (60°C) = 0.0084 atm.

From equations [7] and [8] the Cl_2(aq) and H_2CO_3 activities are: $p\{Cl_2(aq)\}$ (25°C) = 1.23; $p\{H_2CO_3\}$ (25°C) = 3.47; $p\{Cl_2(aq)\}$ (60°C) = 1.90; $p\{H_2CO_3\}$ (60°C) = 3.88.

According to Sherrill and Izard (5), Cl_2(aq) in concentrated NaCl solutions forms Cl_3^- ions to such a great extent that they cannot be neglected. The equilibrium constant $\{Cl_3^-\}/\{Cl^-\}\mathfrak{p}_{Cl_2}$ is 0.01 atm^{-1} at 25°C and hence $p\{Cl_3^-\}$ (25°C) = 1.4.

From equations [1–5] logarithms of the activities of the substances can be obtained as functions of $p\{H_3O^+\}$, i.e., of pH:

$$p\{HClO\} = -pH - p\{Cl^-\} + p\{Cl_2(aq)\} + pK_1 \quad \text{(from [1])}$$

$$p\{ClO^-\} = -2pH - p\{Cl^-\} + p\{Cl_2(aq)\} + pK_1 + pK_s \quad \text{(from [1] and [3])}$$

$$p\{ClO_3^-\} = -6pH - 5p\{Cl^-\} + 3p\{Cl_2(aq)\} + pK_2 \quad \text{(from [2])}$$

$$p\{HCO_3^-\} = -pH + p\{H_2CO_3\} + pK_{s1} \quad \text{(from [4])}$$

TABLE I

Temp	25°C			60°C		
NaCl conc	250 g/l	310 g/l	Mean value	250 g/l	310 g/l	Mean value
a	5.16	5.26	5.2	5.50	5.60	5.6
b	12.52	12.62	12.6	12.59	12.69	12.6
c	17.83	18.33	18.1	19.64	20.14	19.9
d	9.81	9.81	9.8	10.14	10.14	10.1
e	20.06	20.06	20.1	20.26	20.26	20.3

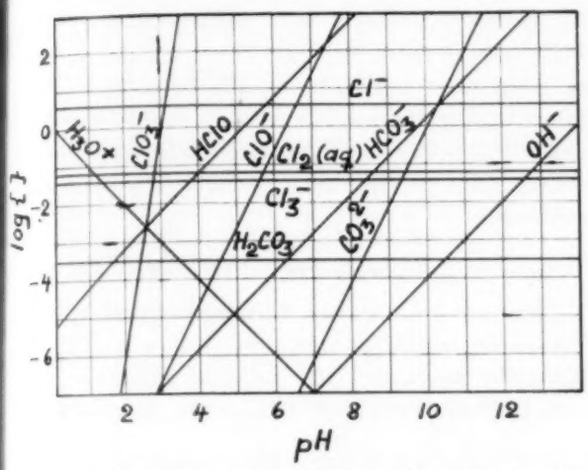

FIG. 1. Logarithms of activities in mole l^{-1} for the substances considered as a function of *p*H at 25°C.

$$p\{CO_3^{=}\} = -2pH + p\{H_2CO_3\} + pK_{s1} + pK_{s2} \quad \text{(from [4] and [5])}$$

If the constant terms of modified equations [1–5] are combined, we obtain:

$$p\{HClO\} = -pH + a$$

$$p\{ClO^-\} = -2pH + b$$

$$p\{ClO_3^-\} = -6pH + c$$

$$p\{HCO_3^-\} = -pH + d$$

$$p\{CO_3^{=}\} = -2pH + e$$

The values of the constants are given in Table I.

In practical operation, uncertainty of a *p*H measurement appears in the first decimal and, according to Table I, the influence of decreasing salt concentration during electrolysis is of the same order of magnitude as uncertainty of a measured *p*H value. Therefore, a mean value has also been tabulated, which will apply to the whole concentration range of a cell.

Table I shows that chlorate activity will be mostly influenced by a temperature change, and that all activities of the chlorine and carbon dioxide systems will decrease with increasing temperature at constant *p*H.

Fig. 1 and 2, giving the logarithm of the activity of each dissolved substance vs. *p*H, were drawn

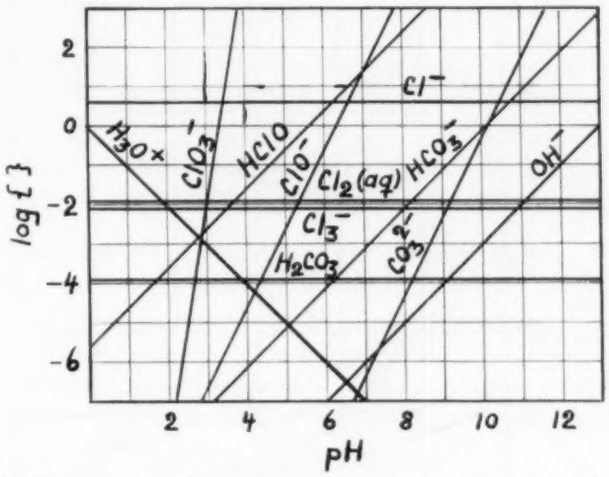

FIG. 2. Logarithms of activities in mole l^{-1} for the substances considered as a function of *p*H at 60°C.

using mean values of the constant terms at 25° and 60°C, respectively.

The Cl_3^- line of Fig. 2 is drawn with the assumption that the relation $\{Cl_3^-\}/\{Cl_2(aq)\}$ is constant between 25° and 60°C. Then $p\{Cl_3^-\}$ (60°C) = 2.1.

In the figures the OH^- ion activity was drawn as calculated from the equation:

$$p\{OH^-\} = -pH + pK_v \qquad [10]$$

in which pK_v (25°C) = 14.00 and pK_v (60°C) = 13.02 (14).

A Practical Equilibrium Diagram

The alkaline part of the Figures 1 and 2 can evidently never become actual, since $[Na^+] \simeq [Cl^-]$ and the solution must be electrically neutral at a sufficient distance from the electrodes. (Square brackets indicate concentration in mole/l.)

Fig. 3 was drawn using concentrations instead of activities at 60°C. It was then assumed that activity coefficients of the ions are constant within the *p*H range and equal to 0.9. This figure is approximate and was extrapolated from a diagram applying at 25°C (12). According to an investigation of the solubility of chlorine in various salt solutions at room temperature (5), the activity coefficient of $Cl_2(aq)$ is about 4 in this concentration range. This value was also used at 60°C in Fig. 3 for both $Cl_2(aq)$ and HClO, which also constitutes an approximation.

In Fig. 3, the *p*H range greater than 5 and less than 1 was excluded, as well as substances whose concentrations are smaller than 1 mmole/l at *p*H 1–5. The water concentration was also calculated from specific gravity of the solution at 60°C, 1.150 with 280 g/l NaCl (15). The equations belonging to Fig. 3 are:

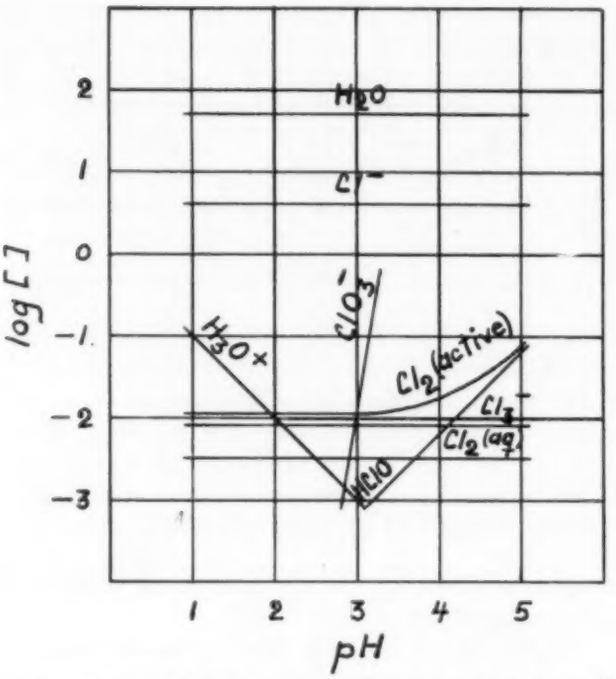

FIG. 3. Logarithms of concentrations in mole l^{-1} for the substances considered as a function of *p*H at 60°C.

$$p[H_3O+] = pH + \log 0.9 \simeq pH$$

$$p[Cl^-] = -0.6 + \log 0.9 \simeq -0.6$$

$$p[Cl_2(aq)] = 1.9 + \log 4 \simeq 2.5$$

$$p[Cl_3^-] = 2.1 + \log 0.9 \simeq 2.1$$

$$p[HClO] = -pH + 5.6 + \log 4 \simeq -pH + 6.2$$

$$p[ClO_3^-] = -6\,pH + 19.9 + \log 0.9 \simeq -6pH + 19.9$$

$$p[H_2O] = -\log \frac{1150 - 280}{18} \simeq -1.7$$

Furthermore, the figure contains a curve giving the concentration of "active chlorine," defined by the expression:

$$[Cl_2(active)] = [Cl_2(aq)] + [Cl_3^-] + [HClO] \quad [11]$$

The curve obtained for active chlorine agrees very well with an experimentally determined curve giving the concentration of active chlorine as a function of *p*H in concentrated, chlorine-saturated NaCl solutions. This agreement decreases the uncertainty introduced by use of approximate activity coefficients and the $\{Cl_3^-\}/\{Cl_2(aq)\}$ relation at 60°C. Thus, Brännland (16) obtained the values shown in Table II at 65°C, 0.995 atm total pressure, and 310 g/l NaCl.

If sodium ion concentration is known, electrolyte composition and *p*H are defined by the condition of electrical neutrality:

$$[Na^+] + [H_3O^+] = [Cl^-] + [Cl_3^-] + [ClO_3^-] \quad [12]$$

TABLE II

*p*H	1.20	4.00	4.35	4.45
log Cl_2 (active)	−2.07	−1.78	−1.51	−1.49

Fig. 3 shows that the chlorate equilibrium concentration increases greatly with increasing *p*H. At *p*H values greater than 3.3 this chlorate content is so great that solid phases will form (17). If, for example, the process is operated at *p*H 4, chlorate ions cannot be in equilibrium with other chlorine components of the brine, and chlorate will form continuously.

Chlorate Formation Rate

The rate of chlorate formation from dissolved chlorine is comparatively slow. It has been investigated by Foerster (18), and according to his results chlorate formation follows the reaction:

$$2HClO + ClO^- + 2H_2O \rightarrow ClO_3^- + 2H_3O^+ + 2Cl^- \quad [13]$$

The chlorate formation rate is then proportional to the square of HClO concentration and to the ClO^- concentration:

$$\frac{d[ClO_3^-]}{dt} = k[HClO]^2[ClO^-] \quad [14]$$

in which k is the rate constant and t the time.

Foerster gives the value of $1/t \log [ClO_3^-]_o/[ClO_3^-]$ min^{-1} at 19.5°, 35°, and 49°C and various HClO concentrations. Since, after having been transformed into the natural logarithm system, this expression is equal to $k[HClO]^2$ in equation [14], the rate constant can be calculated: k(19.5°C) = 0.974, k(35°C) = 3.72, and k(49°C) = 13.8 l^2/min $mole^2$. By means of graphical extrapolation with log k as a function of $1/T$, the value k (60°C) = 39 l^2/min $mole^2$ is obtained.

In a mercury cell, chlorate may also be formed electrochemically at the anode and reduced at the cathode. Murray and Kircher (19) analyzed the anolyte and anode gas of American diaphragm cells and calculated various components of the anodic current loss. They reported that the electrochemical chlorate formation below *p*H 4 is of the same order of magnitude as the chemical one expressed in reaction [13] at the same *p*H. According to Foerster (20), the reaction mechanism of electrochemical chlorate formation implies ClO^- discharge and

oxygen formation at the anode. This type of chlorate formation increases with increasing *p*H, but not so much as the chemical one (reaction [13]) which predominates at *p*H values greater than 4 (19).

Since anode reactions are the same in diaphragm and mercury cells, Murray and Kircher's results are applicable also to the latter.

Fig. 2 shows that $\{HClO\} = 2.5 \times 10^{-3}$ and $\{ClO^-\} = 2.5 \times 10^{-7}$ at *p*H 3 and 60°C. If these values are substituted for the corresponding concentrations in equation [14], the chlorate formation rate $d[ClO_3^-]/dt = 6 \times 10^{-11}$ mole/l min is obtained at *p*H 3. At *p*H 4 and *p*H 5 the value is 6×10^{-7} and 6×10^{-3} mole/l/min, respectively.

Thus, the chlorate formation rate is significant only at *p*H values above 4, because of the small content of the chlorate forming substances, HClO and ClO^-, at lower *p*H values.

According to Sand (4) the chlorate decomposition follows the reaction:

$$ClO_3^- + 2H_3O^+ + 2Cl^- \rightarrow 2HClO + ClO^- + 2H_2O \quad [15]$$

which is evidently the inverse reaction to that which Foerster (18) proved for chlorate formation. Sand reported the rate constant of the reaction at 70°C = 0.56×10^{-3} min^{-1}.

If the rate constant is assumed to be increased 2.5 times by a temperature rise of 10°C, and if the values of Fig. 2 for ClO_3^-, H_3O^+, and Cl^- at *p*H 3 are used, the decomposition rate of ClO_3^-, $-d[ClO_3^-]/dt$, is 4×10^{-11} mole/l min at 60°C. This decomposition rate is of the same order of magnitude as the above calculated chlorate formation rate at *p*H 3, i.e., the chlorate concentration is in equilibrium, which agrees with the equilibrium diagrams constructed above.

Contrary to chlorate formation, acid formation occurs instantly (4), and probably the equilibrium concentrations of HCl and HClO are reached even at the first anode which the brine touches.

The result of these calculations of electrolyte composition is verified in the investigations by Murray and Kircher (19).

Anode Process and *p*H of the Brine

Only the substances included in Fig. 3 will be considered.

The desired anode reaction may be separated into an "electrochemical" part:

$$2Cl^- \rightarrow Cl_2(aq) + 2e^- \quad [16]$$

and a "physical" part:

$$Cl_2(aq) \rightarrow Cl_2(g) \quad [17]$$

in which (g) means that the substance is gaseous.

With reference to combined reactions [16] and [17], the anode potential is:

$$e_a = e_1^0 + \frac{RT}{2\mathbf{F}} \ln \frac{\{Cl_2(g)\}}{\{Cl^-\}^2} + f_1(i) \quad [18]$$

in which e_1^0 is the standard potential of reaction [16] and [17], **F** the Faraday constant, and $f_1(i)$ the current density dependent chlorine overvoltage.

Anodic current loss is represented by a number of reactions, which may be divided into two groups: (*a*) "water electrolysis":

$$6H_2O \rightarrow O_2(g) + 4H_3O^+ + 4e^- \quad [19]$$

or with graphite oxidation included:

$$C(s) + 6H_2O \rightarrow CO_2(g) + 4H_3O^+ + 4e^- \quad [20]$$

in which (s) means that the substance is solid, and (*b*) "chloride electrolysis":

$$Cl^- + 2H_2O \rightarrow HClO + H_3O^+ + 2e^- \quad [21]$$

$$Cl^- + 9H_2O \rightarrow ClO_3^- + 6H_3O^+ + 6e^- \quad [22]$$

In the first group of side reactions, irreversible reaction [20] predominates, since the anode gas generally contains about 1% CO_2 and small quantities of O_2 as well as air. This reaction causes not only current loss but also graphite loss.

The anode potential e_a is, according to reaction [19]:

$$e_a = e_2^0 + \frac{RT}{4\mathbf{F}} \ln \frac{\{O_2(g)\}\{H_3O^+\}^4}{\{H_2O\}^6} + f_2(i) \quad [23]$$

in which e_2^0 is the standard potential of reaction [19], and $f_2(i)$ represents the current density dependent polarization.

e_a is fixed by equation [18], and is evidently independent of *p*H of the solution. Since $\{H_2O\}$ is constant, the following equation is obtained at constant current density and temperature, provided that f_2 is independent of variations in brine composition:

$$d \log \{O_2(g)\} = 4\, d\, pH \quad [24]$$

As $\{O_2(g)\}$ is proportional to $\mathfrak{p}_{CO_2}$ in the gas phase, carbon dioxide content of the anode gas and graphite loss of the cell increase with *p*H according to the equation:

$$d \log \mathfrak{p}_{CO_2} = 4\, d\, pH \quad [25]$$

In the "chloride group" current loss can be partly recovered as chlorine gas by brine dechlorination after electrolysis. Furthermore, since no graphite loss or contamination of the gas phase is caused

TABLE III

pH of anolyte	Anodic current loss, s_a%	log (s_a − 1.5)
3.0	1.8	−0.5
3.5	2.6	+0.1
4.0	5.1	+0.6
4.5	15.8	+1.2

by this group of reactions, it may be regarded as less harmful than the former.

By forming corresponding expressions for e_a for reactions [21] and [22], and by keeping all quantities constant except {HClO}, $\{ClO_3^-\}$, and $\{H_3O^+\}$, the following relations between these variables are obtained:

$$d \log \{HClO\} = d\ pH \qquad [26]$$

and

$$d \log \{ClO_3^-\} = 6\ d\ pH \qquad [27]$$

These equations have already been derived in equilibrium calculations above. It has also been shown that chlorate formation will not always reach equilibrium in the cell.

If the logarithm of equation [14] is taken and $p[HClO]$ and $p[ClO^-]$ vs. pH inserted, the following expression is obtained:

$$\log \frac{d[ClO_3^-]}{dt} = 4pH + \text{a constant} \qquad [28]$$

and after differentiating:

$$d \log \frac{d[ClO_3^-]}{dt} = 4\ d\ pH \qquad [29]$$

Evidently, the chlorate formation rate increases with pH in a similar way as equilibrium activities.

The above calculations demonstrate that anodic current efficiency increases with decreasing pH of the anolyte. Composition of the latter is given by the equilibrium diagram in Fig. 3. This result is not affected by mechanisms of the particular reactions, e.g., if hypochlorite and chlorate are formed "chemically" through internal electron change or "electrochemically" through electron delivery to the anode.

This result is also confirmed by Murray and Kircher (19). Under constant experimental conditions, they obtained the relation shown in Table III between anodic current loss, s_a, and pH of the anolyte.

Current loss due to the anolyte content of $Cl_2(aq)$ and Cl_3^-, which are entirely lost in the diaphragm process, and current loss due to sulfate content of technical brine are both independent of pH. If 1.5% is subtracted from total current loss as a correction for pH independent current losses, the logarithm of the remaining pH dependent current loss will become a linear function of pH, which actually satisfies relations derived above between losses and pH. This is demonstrated in the last column of Table III

In the above derivation of equilibrium composition of the electrolyte, certain constant chlorine and carbon dioxide pressures in the gas phase were assumed. Composition of the latter is, of course, changed with the current efficiency, but at a moderate change of current efficiency, change of chlorine pressure is not so great that derived equilibrium diagrams are affected. As to the carbon dioxide system, it has been shown that its presence in the electrolyte may be neglected.

Cathode Process and pH of the Brine

Since, in dilute mercury solutions, sodium is probably dissociated into sodium ions and free electrons, the desired cathode process implies merely a phase boundary passage by sodium ions:

$$Na^+(aq) \rightarrow Na^+(Hg) \qquad [30]$$

Simultaneously, the mercury cathode is supplied with electrons externally:

$$e^- \rightarrow e^-\ (Hg) \qquad [31]$$

in which (Hg) means that the substance is dissolved in mercury.

According to this way of regarding the reactions, which was used by Brönsted (21) in studies of reaction mechanism for dissolution of metals in acids, sodium ions participate only in a "physical" reaction at the cathode, which is probably completely reversible. Since other current efficiency decreasing cathode reactions also take place, reaction [31] must occur a little faster than reaction [30]. The rate difference is defined by loss reactions, which may be divided into two groups as for the anodic ones, "water electrolysis":

$$2e^-(Hg) + 2H_2O \rightarrow 2OH^- + H_2(g) \qquad [32]$$

and "chloride electrolysis":

$$2e^-(Hg) + Cl_2(aq) \rightarrow 2Cl^- \qquad [33]$$

$$2e^-(Hg) + ClO^- + H_2O \rightarrow Cl^- + 2OH^- \qquad [34]$$

$$6e^-(Hg) + ClO_3^- + 3H_2O \rightarrow Cl^- + 6OH^- \qquad [35]$$

Cathode reactions are written in alkaline form, as the liquid film near the mercury is alkaline, which may be calculated from the hydrogen overvoltage and the electrode potential electrolyte/amalgam.

The cathode potential, e_k, is -1.8 volts under conditions prevailing in a mercury cell operated with 30 amp/dm^2 (22). With reference to reaction [32] it may be written:

$$e_k = e_3^0 + \frac{RT}{2F} \ln \frac{\{H_2O\}^2}{\{OH^-\}^2\{H_2(g)\}} - f_3(i) \qquad [36]$$

in which e_3^0 is the standard potential of reaction [32] and $f_3(i)$ the hydrogen overvoltage.

According to Glasstone (23), hydrogen overvoltage is independent of the *p*H of the solution. Tafel (24) reported that overvoltage increases with current density according to the formula $f_3(i) = a + b \ln i$, a and b being constants. If the cell gas contains, for example, 0.5% H_2 and the cell is operated with 30 amp/dm^2 of mercury surface, the current density of the hydrogen discharge is about 1.5 ma/cm^2. With this current density the hydrogen overvoltage should be 0.9–1.0 volt at room temperature according to Knobel (25). Glasstone (23) reported that hydrogen overvoltage on mercury decreases with increasing temperature, 2.1 mv/°C, so the lower figure is assumed to apply at 60°C. It is also assumed to apply to mercury containing a little sodium.

The standard potential e_3^0 is -0.83 volt at 25°C (26), and, after correction for temperature change of the water constant K_w (14), a value of -0.86 is obtained for 60°C.

If hydrogen is assumed to be discharged as gas bubbles on mercury, and if $\{H_2O\} = 1$, the following equation is obtained at 60°C, from equation [36]:

$$-1.8 = -0.86 + \frac{0.066}{2} \log \frac{1}{\{OH^-\}^2} - 0.9$$

which gives the result $p\{OH^-\} \simeq 0$, or at 60°C *p*H $\simeq 13$.

The value is, of course, very uncertain, since uncertainty in overvoltage and probably also in cathode potential amounts to some tenths of a volt.

However, it may be concluded that the cathode film of a mercury cell is more alkaline than the bulk of the electrolyte, which is represented in Fig. 3, and that *p*H of the film is certainly greater than 7. Moreover, the value changes along the perpendicular through the cathode film to the mercury surface, and is therefore dependent on the point of the cathode potential measurement.

In a series of kinetic studies on decomposition of sodium amalgam in various solutions, Brönsted and Ross Kane (21) found that the decomposition rate increased greatly with decreasing *p*H. The amalgam contained 0.055% Na, and the lowest *p*H was 7.5, under which value the reaction rate was too fast to be measured reliably. This agrees with the above estimation of alkalinity of the cathode film.

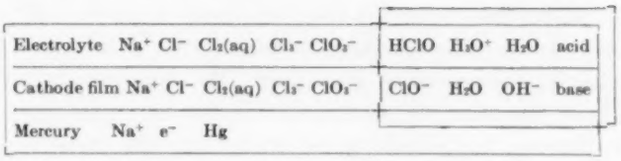

FIG. 4. Sketch of the composition of the bulk of the electrolyte, the cathode film, and the mercury phase.

As with the anode, the following equation is obtained by differentiating equation [36] with all variables constant, except $\{OH^-\}$ and $\{H_2(g)\}$:

$$d \log \{H_2(g)\} = 2\, d\, p\, \{OH^-\} = -2\, d\, pH \qquad [37]$$

Reactions [34] and [35] also become faster as *p*H of the cathode film decreases, while reaction [33] which implies that the desired anode product is consumed at the cathode is independent of *p*H.

The discussion shows that cathodic current efficiency increases with increasing *p*H of the cathode film.

Interaction between Anodic and Cathodic Loss Reactions

Owing to alkalinity of the cathode film and high hydrogen overvoltage on mercury, reaction [30] predominates over reaction [32], and the mercury process is rendered possible. The process may consequently be disturbed by substances which neutralize the cathode film or catalyze hydrogen discharge by decreasing hydrogen overvoltage. Among other substances, vanadium, chromium, and molybdenum belong to this latter group (27). However, such contaminated systems are outside the scope of this investigation.

It has been shown that a certain alkalinity of the film near the mercury is essential for the process. At *p*H values between that of the bulk of the electrolyte and that of the cathode film, HClO is protolyzed to ClO^-. A qualitative representation of the composition of the acid electrolyte, the alkaline cathode film, and the mercury is given in Fig. 4.

Since in the electric field OH^- ions migrate from the cathode film, and H_3O^+ ions migrate toward the cathode film, OH^- ions of the film thus lost must evidently be replaced. This is done according to reaction [32] or by chlorine reduction as in reactions [34] and [35]. The resulting current loss can never be avoided, and consequently current efficiency can never reach 100%.

With a knowledge of migration rate, the magnitude of this current loss can be estimated. If a diaphragm between the acid electrolyte and alkaline

cathode film is imagined, $[OH^-]\cdot u_-\cdot X$ mole OH^- ions/sec migrate through 1 dm^2 of the diaphragm, and in the opposite direction, $[H_3O^+]\cdot u_+\cdot X$ mole H_3O^+ ions/dm^2 sec, in which u is the ionic mobility in dm/sec at the field strength 1 v/cm and X is the field strength in v/cm. At 60°C the mobility of OH^- ions is 33×10^{-5} dm/sec v/cm, and that of H_3O^+ ions 52×10^{-5} dm/sec v/cm (28). These ionic mobilities must be corrected because viscosity of the salt solution is higher than that of pure water. According to Angel (29), the change is defined by the formula:

$$u_2 = u_1(\eta_1/\eta_2)^m \qquad [38]$$

in which m is a constant = 0.614 for H_3O^+ ions and 0.718 for OH^- ions, and η the viscosity. If the viscosity of water at 60°C, 0.469 centipoise (30), is inserted for η_1 and the viscosity of a 25% NaCl solution at the same temperature, 1.11 centipoise (31), for η_2, we obtain for OH^-, $u_- = 18\cdot10^{-5}$ dm/sec v/cm, and for H_3O^+, $u_+ = 31 \times 10^{-5}$ dm/sec v/cm. The specific conductivity of the salt solution at 60°C is 0.43 ohm^{-1} cm^{-1} (15). With the current density i amp/dm^2 the field strength X is $i/43$ v/cm.

The pH of the alkaline side being assumed = x, that of the acid side = y, and the current loss caused by these ion migrations = s_k, the following equation is obtained, since i amp/dm^2 corresponds to $i/96500$ moles of electrons $sec^{-1}dm^{-2}$ and since $pK_w(60°C) = 13$ (14) (provided that the activity coefficients = 1):

$$i\cdot s_k/96500 = (i\cdot 18\cdot 10^{-5}\cdot 10^{x-13}/43) + (i\cdot 31\cdot 10^{-5}\cdot 10^{-y}/43) \qquad [39]$$

This formula gives the minimum cathodic current loss for different pH values of electrolyte and cathode film at 60°C. It is independent of current density.

For example, pH 3 and pH 11 inserted in equation [39] give $s_k = 0.5\%$, pH 3 and pH 10 give $s_k = 0.1\%$, etc.

By stirring the electrolyte, more acid than that corresponding to these electrolytic migration rates may penetrate into the cathode film. It is evidently important that the streaming state of the cathode film should be laminar. Turbulence of the cathode film decreases current efficiency since alkali neutralized thereby must be re-formed. Furthermore, chlorine diffuses more easily into the cathode film and reacts according to equations [33–35]. Solid particles floating on the mercury act as stirrers on the cathode film and thus interfere with the process.

This effect may possibly be the reason why the vertical cell built by the Germans during World War II in order to save floor space never gave the same current efficiency as the traditional horizontal cell (32).

According to Fig. 4, the acid/base couple HClO/ClO^- is present at the boundary between electrolyte and cathode film. HClO is instantly protolyzed to ClO^- at a pH between that of the electrolyte and that of the cathode film. Owing to the stirring influence of the anode gas bubbling around the anodes at only a few millimeters distance from the cathode film, HClO may easily reach the reaction zone. If the effect of H_3O^+ migration toward the cathode in the electric field is neglected, HClO should decompose the cathode film in the same manner as H_3O^+.

Consequently, cathodic current efficiency decreases both with increasing H_3O^+ and increasing HClO concentration in the electrolyte. According to Fig. 3, concentration of (H_3O^+ + HClO) reaches a symmetrical minimum at pH 3. Provided that a certain HClO concentration in the electrolyte has about the same neutralizing effect on the cathode film as a like concentration of H_3O^+, which has been only argumentatively derived above, the cathodic current efficiency reaches a symmetric maximum at about pH 3.

This pH value, at which the acid concentration reaches its minimum, only changes by a few tenths of a unit within the generally applied temperature range, which is shown by a comparison of Fig. 1 and 2.

Since anodic current efficiency decreases with increasing pH, the pH of the electrolyte should not exceed this value, pH 3, by very much.

Unfortunately, this result cannot be illustrated by any electrolysis experiments, but it is known from practical experience that H_2 content of the gas generally increases with both exceptionally high alkalinity and acidity of the feed brine. However, the scientific basis is lacking, since these matters have been investigated very little. Probably, catalytic phenomena also have an influence.

At pH 3 and 60°C the equilibrium value of log $[ClO_3^-]$ is −1.9, i.e., the chlorate concentration is 1.3 g/l $NaClO_3$. Under these conditions chlorate formation and decomposition rates are small. Above pH 4 in the electrolyte, chlorate formation begins to be very strong, which has been shown in calculation of the electrolyte composition above. It is known practically that if mercury cells are supplied with alkaline brine, chlorate may accumulate in the system, unless a special device for chlorate decomposition is installed. This was the case in the so-called IG process (33). Chlorate is not harmful to the process, but, since chlorate accumulation in

the brine must be prevented, construction and operation costs of the plant are increased if the brine supplied is alkaline. Because of chlorate formation, *p*H of the brine should consequently not exceed *p*H 4, which is reconcilable with the condition that due to other current losses *p*H of the electrolyte should not exceed *p*H 3 very much.

Discussion of Most Suitable Composition for Feed Brine

According to the foregoing discussion, feed brine ought to have such a composition that *p*H of the bulk of the electrolyte, which in this case may be represented by the depleted brine, is less than *p*H 3. As demonstrated by the reaction formulas, anodic current loss implies acid formation, and the cathodic one alkali formation. Composition of feed brine is consequently dependent on all factors which affect current efficiency when a certain *p*H of the electrolyte is desired.

Experience shows that, in general, depleted brine has more than 1 g/l chlorine and *p*H 4 when the feed brine is "soda alkaline." In most cases it is sufficient to lower *p*H of the feed brine, after the precipitation of $CaCO_3$ and $Mg(OH)_2$ in alkaline solution, to about 7 in order to obtain less than 1 g/l chlorine and *p*H 3 in the electrolyte.

It should be noted that not only OH^- but all the basic components of the feed brine, which consume protons during the *p*H decrease which occurs during the saturation with chlorine in the cell, define the alkalinity of the brine.

If, for instance, composition of the feed brine is: 0.10 g/l chlorine, 0.30 g/l Na_2CO_3, 0.040 g/l NaOH, then at 25°C and *p*H 11 the molar concentrations are: $[ClO^-] = 0.0014$, $[CO_3^=] = 0.0028$, $[OH^-] = 0.0010$, and the total alkalinity $= [ClO^-] + 2[CO_3^=] + [OH^-] = 0.0080$ mole/l. This corresponds to a chlorine and carbon dioxide free solution with *p*H 12 at 25°C.

This explains why hydrogen content of the gas generally increases with increasing chlorine concentration in the feed brine, when it is alkaline. Chlorine content in the brine increases alkalinity which might previously have been near the allowable limit.

If the process is operated at *p*H 3 under constant experimental conditions with good results, and if the feed brine is becoming more acid, then acid formation at the anode decreases, and base formation at the cathode increases, which reactions both counteract the effect of the decreasing *p*H of the feed brine. If, on the other hand, the brine is getting more alkaline, acid formation at the anode increases, and also base formation at the cathode, because then the HClO concentration of the electrolyte increases. In this case it is evidently not certain that the influence of change in brine composition is counteracted by the cell. If OH^- formation at the cathode should predominate over H_3O^+ formation at the anode, HClO content of the electrolyte would increase and loss reactions "catalyze" themselves, until the extreme case is reached, in which the cell works as a chlorate or hypochlorite cell and the gas phase contains hardly any chlorine and only hydrogen and carbon dioxide. Therefore, too alkaline brines may seem to be more hazardous than too acid ones.

In a plant with brine purification it is thus necessary to be sure that the sum $[OH^-] + 2[CO_3^=] + [HCO_3^-] + [ClO^-]$ is not too great in the purified solution which is supplied to the electrolysis system.

On the other hand, in a plant which is operated with pure salt and no unit processes other than electrolysis and resaturation, Fig. 3 is applicable. It is then necessary to be sure only that chlorine and chlorate concentrations are below a certain limit. If this is exceeded, hydrochloric acid should be supplied to the system. If *p*H of the solution should become too low, the necessary quantity of alkali is produced in the cells.

Summary

1. In chlorine-caustic electrolysis the following substances and ions, belonging to water, chlorine, and carbon dioxide systems, cannot be neglected in study of the electrolyte: H_2O, H_3O^+, Cl^-, Cl_2, Cl_3^-, HClO, and ClO_2^-.

2. Concentration of active chlorine in the brine is the sum of Cl_2, Cl_3^-, and HClO concentrations. In this sum, Cl_3^- concentration predominates below *p*H 4, and HClO concentration above *p*H 4. The former is independent of *p*H of the electrolyte, and constant at a given temperature and chlorine pressure. The latter concentration increases with increasing *p*H. Equilibrium concentrations are reached instantaneously.

3. Concentration of acid in the brine is the sum of H_3O^+ and HClO concentrations. The H_3O^+ concentration predominates below *p*H 3, and the HClO concentration above this value. The sum of these concentrations reaches a minimum at *p*H 3. Equilibrium concentrations are reached instantaneously.

4. Chlorate equilibrium concentration of the brine increases greatly with increasing *p*H. Equilibrium concentration is *not* reached instantaneously. Above *p*H 3.3, it is so high that the system becomes heterogeneous at the high NaCl concentration of a mercury cell. The chlorate formation rate increases

with increasing *p*H but does not become noticeable until *p*H 4. The chlorate decomposition rate increases with decreasing *p*H at a given chlorate concentration, and is slight in the electrolyte.

5. Anodic current efficiency increases with decreasing *p*H of the electrolyte.

6. The cathode film near the mercury is alkaline, i.e., its *p*H is greater than 7.

7. Cathodic current efficiency increases with increasing *p*H of the cathode film.

8. Cathodic current efficiency cannot reach 100% owing to reactions between the acid electrolyte and alkaline cathode film.

9. Agitation of the cathode film interferes with the process.

10. Cathodic current efficiency passes a maximum at *p*H 3 of the electrolyte.

11. Highest possible current efficiency with respect to chlorine and caustic is not obtained if *p*H of the bulk of the electrolyte exceeds 3.

12. All bases in the feed brine which are protolyzed during *p*H decrease in the cell define proper composition of the feed brine. The sum of the concentrations of these bases (OH^-, $CO_3^=$, HCO_3^-, and ClO^-) should not exceed a certain value.

Acknowledgment

The author wishes to express his deep appreciation to Dr. Ragnar Söderquist, Stora Kopparbergs Bergslags AB, for permission to publish results of the work which was carried out at this company. He is also greatly indebted to Rolf Brännland, the Royal Institute of Technology, Stockholm, for helpful criticism and discussions when writing the manuscript, and to the State Council of Technical Research for a grant making translation possible.

Any discussion of this paper will appear in a Discussion Section to be published in the June 1955 issue of the JOURNAL.

References

1. R. TAUSSIG, *Trans. Faraday Soc.*, **5**, 258 (1909-1910).
2. N. J. JOHNSON, *Trans. Electrochem. Soc.*, **86**, 127 (1944).
3. A. A. JAKOWKIN, *Z. physik. Chem.*, **29**, 613 (1899).
4. J. SAND, *ibid.*, **50**, 465 (1904).
5. M. S. SHERRILL AND E. F. IZARD, *J. Am. Chem. Soc.*, **53**, 1667 (1931).
6. J. SAND, *Z. physik. Chem.*, **48**, 610 (1904).
7. D. A. MACINNES AND D. BELCHER, *J. Am. Chem. Soc.*, **55**, 2630 (1933).
8. D. A. MACINNES AND D. BELCHER, *ibid.*, **57**, 1683 (1935).
9. R. P. WHITNEY AND J. E. VIVIAN, *Ind. Eng. Chem.*, **33**, 741 (1941).
10. J. L. GAY-LUSSAC, *Ann. chim. phys.*, [3], **7**, 124 (1843).
11. C. D. HODGMAN, "Handbook of Chemistry and Physics," 33rd ed., p. 1480, Chemical Rubber Publishing Co., Cleveland (1951).
12. R. ROBINSON, *J. Am. Chem. Soc.*, **57**, 1163 (1935).
13. C. D. HODGMAN, *op. cit.*, p. 2033.
14. H. S. HARNED AND B. B. OWEN, "The Physical Chemistry of Electrolytic Solutions," 2nd ed., p. 485, Reinhold Publishing Corp., New York (1950).
15. L. DEMOLIS, *J. chim. phys.*, **4**, 528 (1906).
16. R. BRÄNNLAND, private communication.
17. F. WINTELER, *Z. Elektrochem.*, **7**, 360 (1900).
18. F. FOERSTER, *J. prakt. Chem.*, **63**, 141 (1901).
19. R. L. MURRAY AND M. S. KIRCHER, *Trans. Electrochem. Soc.*, **86**, 83 (1944).
20. F. FOERSTER, *Trans. Electrochem. Soc.*, **46**, 23 (1924).
21. J. N. BRÖNSTED AND N. L. ROSS KANE, *J. Am. Chem. Soc.*, **53**, 3624 (1931).
22. V. DE NORA, *This Journal*, **97**, 346 (1950).
23. S. GLASSTONE, *J. Chem. Soc.*, **125**, 2646 (1924).
24. J. TAFEL, *Z. physik. Chem.*, **50**, 641 (1904).
25. M. KNOBEL, *J. Am. Chem. Soc.*, **46**, 2613 (1924).
26. C. D. HODGMAN, *op. cit.*, p. 1500.
27. G. ANGEL AND T. LUNDÉN, *This Journal*, **99**, 435 (1952).
28. C. D. HODGMAN, *op. cit.*, p. 2153.
29. G. ANGEL, *Z. physik. Chem.*, **170**, 81 (1934).
30. C. D. HODGMAN, *op. cit.*, p. 1830.
31. J. H. PERRY, "Chemical Engineers' Handbook," 3rd ed., p. 373, McGraw-Hill Book Co., New York (1950).
32. FIAT Final Report No. 817, "Vertical Mercury Chlorine Cells," p. 34, H.M. Stationery Office, London (1946).
33. FIAT Final Report No. 816, "Horizontal Mercury Chlorine Cell," p. 62, H.M. Stationery Office, London (1946).

Some Observations on the Kroll Process for Titanium[1]

F. S. Wartman, Don H. Baker, J. R. Nettle, and V. E. Homme

U. S. Department of the Interior, Bureau of Mines, Boulder City, Nevada

ABSTRACT

A series of small-scale Kroll process reductions, carried to varying degrees of completion, were opened and examined to obtain information concerning the mechanism of the reduction. Experiments made to determine the cause of zonal variations of hardness in the crude sponge made by the Kroll process indicate this effect is due largely to impurities in the magnesium.

Introduction

Since the first appearance in this country of a published description (1) of the method of producing titanium by magnesium reduction, the process has been actively investigated (2–8). As a result, a number of modifications to the process as originally described have been developed or suggested. Two of these (3, 4) are: (*a*) elimination of the molybdenum lining for the reaction chamber, as large molybdenum-lined reactors would have been prohibitively expensive; and (*b*) provision for removal of the by-product magnesium chloride during and immediately after reduction to facilitate the rate of reduction, obtain up to 90% of the magnesium chloride in pure concentrated form, and simplify later purification of the product of reduction.

Outline of the Process

The technique now in use at the pilot plant operated by the Bureau of Mines is described here briefly.

The requisite quantity of magnesium ingots, previously pickled and dried, are placed in an empty reaction chamber made of mild steel; the lid is sealed in place by a weld having only slight penetration. Then the chamber is placed in the furnace, the various supply lines are attached, and the air in the reaction chamber is replaced with helium. Finally, after the temperature of the furnace has been raised to 850°C and held there long enough to melt the magnesium, a stream of liquid titanium chloride is allowed to fall on the hot magnesium until enough titanic chloride has been added to react with about 85% of the magnesium according to the equation:

$$TiCl_4\ (l) + 2Mg\ (l) = 2MgCl_2\ (l) + Ti\ (s) \quad (I)$$

The reaction is strongly exothermic and the temperature in the reaction zone is held at 900°–1050°C by suitable adjustment of the fuel input to the furnace and the rate of adding titanic chloride to the reactor. At intervals magnesium chloride is drawn off in a molten form; 85–90% of the total amount formed is removed in this manner. After reduction has been completed and the reaction chamber has been cooled to room temperature, the cover is removed by grinding off the weld, and the product is removed by mounting the open chamber in a large lathe and boring out the reaction mass. A 0.5-in. thick layer is always left on the wall and bottom of the chamber to serve as a protective lining. The opened reaction chamber must be handled in a room with a very dry atmosphere to lessen absorption of moisture by the hygroscopic $MgCl_2$ left in the mass. The water would react with the titanium when it was heated in later steps of the process. Chips of impure titanium, obtained by the boring, are loaded into retorts and heated at 900°C in a high vacuum to volatilize the residual magnesium and magnesium chloride, leaving the pure titanium, in the form of spongy lumps, as a residue.

Observations on the Mechanism of Titanium Reduction

Two interesting phenomena were observed when this operating technique was used: (*a*) titanium was obtained in a connected mass, with a spongelike appearance, which was attached to the walls of the reactor; and (*b*) the hardness of the metal in the mass of sponge produced by reduction varied according to its position in the mass.

Titanic chloride is introduced into the reaction chamber as a free-falling liquid from a pipe directed downward above the center of the bath. Observation has confirmed the probability that at least part of the liquid actually reaches the surface of the bath. Titanium has a density considerably greater than either magnesium or magnesium

[1] Manuscript received January 25, 1954. This paper was prepared for delivery before the Chicago Meeting, May 2 to 6, 1954.

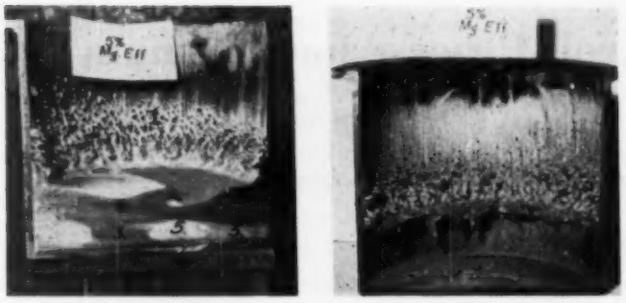

FIG. 1. Bisected chamber after 5% reduction. Left, undistilled segment; right, distilled segment.

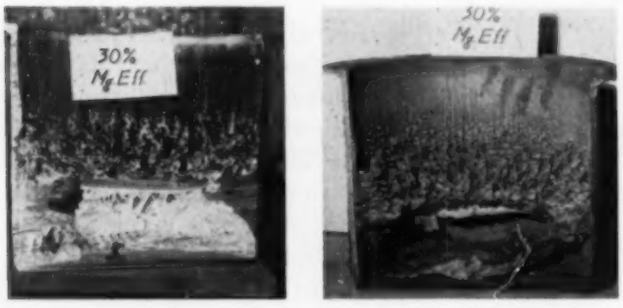

FIG. 2. Bisected chamber after 30% reduction. Left, undistilled segment; right, distilled segment.

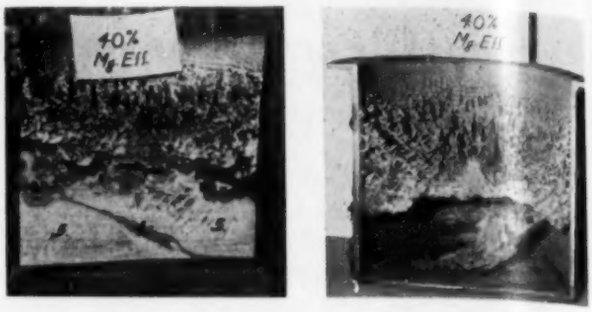

FIG. 3. Bisected chamber after 40% reduction. Left, undistilled segment; right, distilled segment.

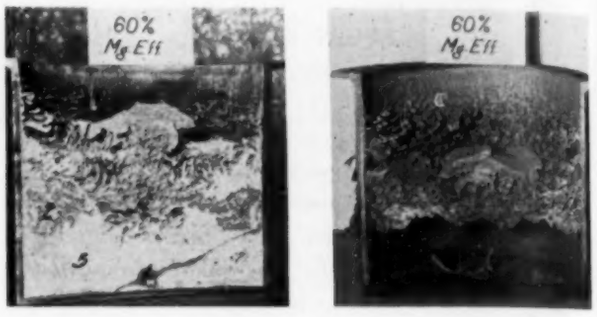

FIG. 4. Bisected chamber after 60% reduction. Left, undistilled segment; right, distilled segment.

chloride, and magnesium and titanic chloride are known to be in contact at the center of the surface of the bath. Therefore, it seems strange that they would not react to form titanium in granular or powder form which, because of its density, might be expected to sink through the bath and be found in a heap on the bottom of the reaction chamber.

A series of seven small reductions was made in an attempt to find an explanation for the apparently anomalous position of the deposit. The reaction chambers were each 25.4 cm in diameter by 25.4 cm high, with a vertical inlet pipe 5 cm in diameter by 91.4 cm long, welded into the center of the cover. They were sand-blasted and partly outgassed by heating in a vacuum for several hours at 900°C. The apparatus was quite similar to that shown in a previous paper (2).

The magnesium charge in each run was approximately 5.7 kg, the temperature at the beginning of the reduction was 800°C, and the rate of addition of titanic chloride after the initial inhibition period was 75 g/min. Thus, the apparatus, operating technique, and physical conditions were as much alike as possible in the different runs. The only variable was the total amount of titanic chloride added, which was 5, 10, 20, 30, 40, 50, and 60%, respectively, of the amount theoretically equivalent to the magnesium added to each run. After each run had been carried to its predetermined degree of completion, it was held at temperature for 1 hr and then allowed to cool. The lid was removed from the cold chamber, and the latter was divided by a vertical cut through the center, so as to expose a cross section of the contents of the chamber. After photographing the exposed face of one half, samples were taken from selected areas for chemical analysis. The locations from which the samples were taken are indicated by appropriate numerals on the photographs of the cross sections. The other halves were placed in a retort, and the volatile constituents such as magnesium and magnesium chloride were removed by vacuum distillation. The location of the residual deposit of titanium was recorded by a photograph. Some of the deposits before and after distillation are depicted in Fig. 1 to 4, and the corresponding analyses are given in Table I.

In Fig. 1, virtually all of the titanium is in the form of a ring attached to the wall of the reactor and extending upward from the point initially marking the juncture of the upper surface of the magnesium with the wall. Analyses show only a little titanium in the magnesium, and after distillation only a small amount of fine, dark powder was found on the bottom. With increasing additions of titanic chloride, the ring of deposited metal continued to extend farther up the wall and also outward toward the center. At some point between 30 and 40% utilization of magnesium, the spongy titanium formed a layer that bridged completely

TABLE I. *Composition of various portions of deposit*

% Magnesium reacted	Analyses, % by weight			Location of sample	
	Mg	Ti	$MgCl_2$	Number on print	Description
5	40	38	22	1	Growths on wall above liquid level
5	94	2.0	0.8	2	Dense metal at top
5	97	1.0	0.6	3	Dense metal at bottom
5	0.2	0.08	98.0	5	$MgCl_2$ phase
30	65	28	7	2	Metal just under surface
30	92	3	tr.	3	Metal at bottom
30	96	4	tr.	4	Metal surrounded by $MgCl_2$
40	48	32	16	1	Metal at surface
40	60	34	7	2	Metal 2″ below surface
40	67	25	66	4	Metallic vein in $MgCl_2$
40	0.8	0.008	94.0	5	$MgCl_2$ phase
60	17	39	40	1	Metal above surface
60	49	43	tr.	2	Metal in lower part of metallic layer
60	32	46	18	4	Metallic vein in $MgCl_2$
60	—	0.03	98	5	$MgCl_2$ phase

across the reactor. From this stage on, the unused magnesium was held in the pores and interstices of the sponge that had already deposited, rather than in a distinctly separate pool. Further growth of the spongy deposit was evidenced by a thickening of the whole layer, with some tendency to formation of a prominence immediately under the end of the feed pipe. In all tests, only a small amount of dark-colored, fine-grained metal was found on the bottom after distillation. The major portion of the weight of the metal produced was in the deposit attached to the walls.

To throw more light on this mode of deposition, another run was made using only 5% of the magnesium. It differed from the first in that short lengths of iron rod 1.27 cm in diameter were welded to the bottom and top of the reaction chamber so as to extend perpendicularly into the reaction space. Of the two welded to the bottom, one extended 1.27 cm above the surface of the magnesium and the other 3.82 cm above the surface. The three welded to the underside of the top terminated 1.27 cm, 2.54 cm, and 3.82 cm, respectively, above the initial level of the free surface of the magnesium. As will be seen from Fig. 5, titanium deposited on the two bars that extended up through the bath, just as it did on the walls. The three bars that extended down from the top remained clean.

If deposition of sponge on the walls had been due either to mechanical splatter or to deposition from a vapor-phase reaction, then metal should have been deposited on the bars extending down

FIG. 5. Cross sections of chamber after 5% reduction. Bars were attached to bottom and top. Left, undistilled segment; right, distilled segment.

close to but not touching the surface of the magnesium. As metal was deposited only on surfaces that passed up through the magnesium, it seems likely that the deposits on the bars extending up through the bath and on the walls were due to a reaction between titanic chloride vapor and a film of magnesium formed on the vertical surfaces by wetting and capillary action. This hypothesis is supported by the known physical properties of the system. Neither magnesium nor titanic chloride is appreciably soluble in magnesium chloride. Therefore it is postulated that when the titanic chloride first comes in contact with the free surface of the magnesium some reaction occurs and some magnesium chloride is formed. This forms a film on the surface that tends to inhibit further reaction. The protective action of such salt films is known and used in the technology of melting, refining, and casting magnesium. On a vertical surface it may be supposed that gravitation causes the magnesium chloride to drain away at least partially, and thus afford better opportunity for contact between titanic chloride and magnesium. This hypothesis may serve as the basis for some interesting predictions concerning the suitability of specific techniques for conducting the reduction. For example, it may be predicted that bringing the two raw materials into contact by allowing droplets of magnesium to fall through the vapor of titanic chloride would not be satisfactory since the droplets would become inactive because of formation of an enveloping film of magnesium chloride.

The tendency to react on vertical rather than horizontal surfaces is probably fundamental, but the nature and location of the deposit formed is affected by the size of the reactor and variations in the manner of operation. For example, Fig. 6 is a view of a reaction mass, contained in a thin iron crucible and cut through the vertical axis. This small reduction run was made for several reasons, one of which was to determine the effect of adding

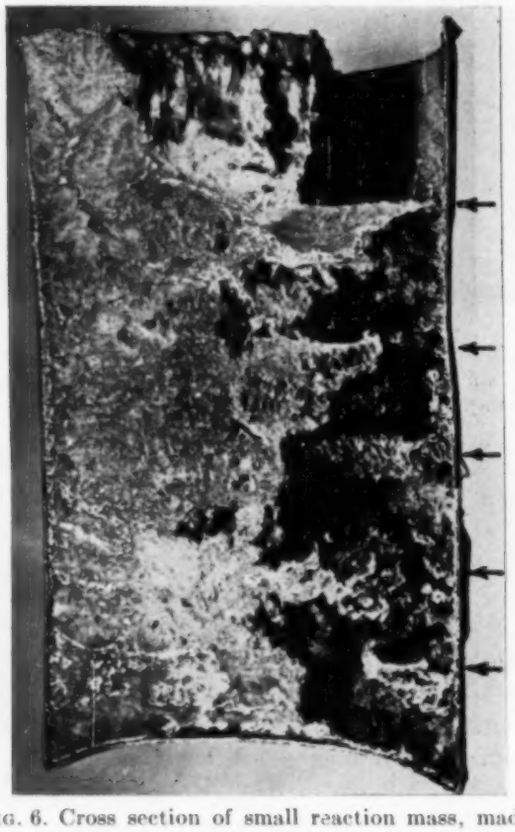

FIG. 6. Cross section of small reaction mass, made to show feasibility of thin disposable liner, multiple additions of magnesium, and tapping of molten magnesium.

the magnesium in increments during the run rather than all at once at the beginning.

About one-fifth of the magnesium was placed in the pot initially, and the rest was added in four increments during the run in the form of small pieces contained in a rubber bag attached to an opening in the top of the reactor. As indicated by the arrows at the right of Fig. 6, the five portions of magnesium resulted in the formation of five separate layers of sponge. These are exposed prominently, because this reaction chamber was removed from the furnace and laid on its side when the reduction was completed. The side at the left then became the bottom, and the still fluid magnesium chloride flowed to the position shown.

If the magnesium chloride had been drawn off so as to keep the zone of reaction at approximately the same level during the reduction, there would have been only a single, dense, thick layer of sponge.

In larger reactors making 91 kg or more of sponge per charge, there is a similar tendency to form a bridge extending upward from the level that originally marked the upper surface of the magnesium. With the greatly increased span, the mechanical strength of the spongy layer is not adequate to allow bridging, and the whole mass collapses to the bottom, particularly when the magnesium chloride is tapped off and its buoyant effect is no longer available to support the bridge of spongy titanium. Since facilities large enough to section and distill large reaction chambers with their contents in place were not available, photographic evidence of the behavior of these large masses cannot be offered.

Observations on the Segregation of Impurities during Reduction

Usual practice at the pilot plant operated by the Bureau of Mines was to mount the opened reaction chamber in a lathe and remove the mass of crude titanium sponge by turning. The chips obtained in this way were treated at 900°C in a high vacuum; as a result of this treatment, hydrogen, magnesium, and magnesium chloride were largely removed by volatilization, and purified spongy titanium remained as the residue. As previously noted, if chips from various parts of the reaction mass were kept segregated during purification, metal produced from chips that came from the center of the reaction mass was freer from impurities and softer than that made from chips that came from the outside and bottom.

Discovery of the cause and a remedy for this condition was of practical importance for several reasons. Variations in hardness and composition of sponge in the same lot introduced difficulties in sampling and testing. Compacts made from such material by powder metallurgy techniques were not uniform in composition and properties. Finally, it was considered desirable to have the best possible quality of primary metal, consistent with reasonable costs of production, in order to allow use of larger quantities of scrap, such as turnings and off-grade sponge, in making new ingots.

Two hypotheses were advanced to explain this tendency to zonal segregation of impurities in the reaction mass: (*A*) during reduction, gases present in the atmosphere around the reaction chamber diffused through the hot mild-steel walls of the chamber and dissolved in the titanium lying closest to the wall on the inside; (*B*) the first titanium formed during the reduction served as a "getter" of the impurities present in the magnesium and on the walls of the reactor and in doing so became hardened. As shown above, the first titanium made is deposited on the walls of the reactor.

The hypothesis that the zonal hardness variations were due to diffusion through the walls of the reactor was tested in two ways. Several types of empty reaction chambers were heated to operating temperature and held there while a slow stream of helium was passed through one side of an electrical thermal conductivity meter, then through the hot chamber, and finally back through the other side

of the meter. After the initial period of outgassing, no contamination of the helium was indicated. Also, small reaction chambers were packed with high grade titanium sponge, outgassed, filled with helium, and then heated for several hours at about 800°C. After the chamber had cooled, it was opened and the sponge removed. While being unloaded, the sponge was segregated into various portions according to position in the chamber during heating. Each portion of sponge was sampled and the sample melted into a small ingot on which the hardness was measured. The hardness of the sponge lying next to the walls of the reactor was not noticeably greater than that of sponge in the center. This also suggests that the zonal variations in hardness were not due to diffusion of gases through the walls of the reactor.

Evidence bearing on the "getter" theory was obtained by making three separate 90-kg Kroll reductions, runs No. 402, 403, and 404, each as nearly alike as possible except in the manner of adding the magnesium. A different reduction chamber was used for each run. Each had been used several times before and had been cleaned and wire-brushed to remove all residues from previous runs. Each pot was finally sealed and treated on the inside with moist hydrogen while at operating temperature. Before cooling, the hydrogen was replaced with helium or argon, and the inert atmosphere was maintained through all subsequent operations until the reduction had been finished and the chamber cooled to room temperature. This prevented readsorption of nitrogen, oxygen, or water vapor on the inner walls of the chamber.

In addition to a variation in the method of adding the magnesium, the technique used in making these three reductions differed in two other ways from that previously described (4). First, the titanium tetrachloride was fed through two stationary pipes introduced into the 5.08 = cm pipes normally used for poking to break up the surface crust on the reaction mass, and the revolving feeder was not used. Second, a long thermocouple with iron protection tube was introduced through a packing gland in the top of the column cover. As the couple could be moved up and down in the packing gland, the temperature could be measured at different levels in the reaction chamber. This was done every half hour until about half of the magnesium had been used. The rate of addition of titanium tetrachloride was adjusted to hold the maximum temperature in the reaction chamber between 950° and 1050°C. The protection tube in moving up and down periodically also took over the function normally performed by the poking rods.

The magnesium used for these three reductions was standard commercial-grade electrolytic magnesium cast in cylindrical billets approximately 40.7 cm long by 10.7 cm in diameter. A typical chemical analysis in percent by weight follows:

Fe	0.05	Mn	0.06
Si	0.003	Al	trace
Ni	0.002	C	0.005–0.12
Cl	0.02		

The billets were cut into three or four pieces and cleaned by pickling, drying, and buffing before use.

In the first run, all the billets were put in the reaction chamber and completely melted before any titanic chloride was added. In the second run about one-fourth of the billets were introduced and melted before starting to feed the titanic chloride. The rest were added at intervals through a lock in proportion to the rate at which titanic chloride was run in. In the third run the charge of clean billets first was melted in a separate chamber under an inert atmosphere and held molten for several hours to allow the solid impurities to settle as much as possible. Then the liquid metal, protected by an inert atmosphere, was siphoned over into the reaction chamber. It was necessary to let the magnesium solidify before the chamber could be disconnected from the siphon and placed in the furnace, but the whole charge was melted again before the reduction was started.

The three reductions were completed and cooled, and the product was recovered by boring and purified by distillation, as described above. In boring, the charge was divided into four lots, approximately as indicated in Fig. 7, and during vacuum distillation each lot from each of the three runs was kept separate.

In studying the data derived from these three reductions as shown in Table II, two points are to be noted particularly. First, the product obtained from runs No. 402 and 404 in which all of the magnesium was added and melted before the reduction started shows very definitely the zonal distribution of hardness and impurities. In contrast, the product of run No. 403 to which magnesium was added in increments during the run shows little variation between the different fractions other than what might be ascribed to normal variations in testing and analysis. Second, the product of run No. 404 in which the magnesium was settled and decanted is noticeably softer than the product of run No. 402 in which the commercial billets were prepared only by cleaning the surface.

By inference, these facts lend strong support to the hypothesis that the zonal variations in hardness are due to the first titanium formed acting as a

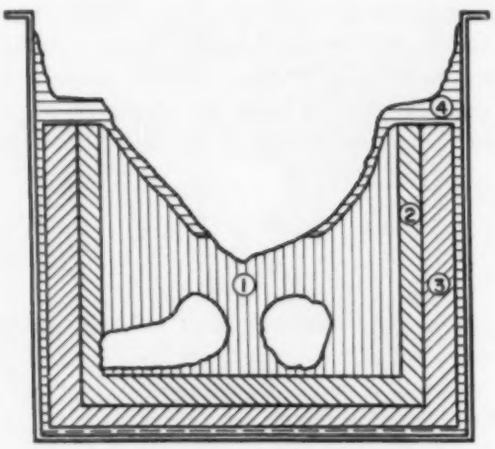

FIG. 7. Sectional diagram showing position of lots 1, 2, 3, and 4 in reaction mass.

getter, since they are to be anticipated on the basis of this hypothesis. The first titanium is deposited on the walls of the reaction chamber just above the upper surface of the magnesium, and magnesium fed by capillary action to the zone of reaction as it rises up the wall and out over the bath must pass through or over this metal. An excellent opportunity is thus afforded for removal of impurities in the magnesium. When magnesium is added during the run, it is already at the surface, is in the reaction zone, and does not have to pass through the metal previously deposited. Consequently, the purifying action does not take place, and all the metal tends to be of about the same grade.

This same effect makes it difficult to produce alloys of titanium of uniform composition by adding the alloying element through the magnesium, if all the magnesium is placed in the reaction chamber before starting the reduction. In one test, an attempt was made to make a titanium alloy containing 1% aluminum by alloying the necessary amount of aluminum with the magnesium before commencing the reduction. Most of the aluminum went into the titanium, which had been deposited first, and only a trace was found in the metal from the center of the reaction mass.

Consideration of the data in Table II also leads to the conclusion that a considerably better grade of titanium could be produced by the Kroll process if magnesium of much higher purity were available in large ingots so as to reduce the amount of impurities both dispersed through the body of the ingot and on the surface. Fraction 1 of run No. 404 indicates the improvement to be expected by this means.

Further inspection of Table II shows that iron, manganese, and oxygen are the principal impurities which would remain after the sponge had been melted to form an ingot. To obtain some idea as to how these impurities affect the hardness of titanium, three series of alloys were made, and the relation

TABLE II. *Data obtained from three special 200-lb reduction runs*

Run No. and description	Lot	Kg	Analyses, % by weight										Brinell hardness
			Fe	Mg	Si	Mn	Ti	N	O	H	Cl	Total of determined impurities	
402. Magnesium in form of commercial billets, all added and melted before starting reduction.	1	36.7	0.03	0.05	0.04	0.03	99.9	0.004	0.062	0.0022	0.06	0.28	110
	2	30.4	0.04	0.06	0.03	0.06	99.85	0.004	0.072	0.0015	0.04	0.31	133
	3	26.7	0.19	< .04	0.03	0.20	99.5	0.003	0.112	0.0026	0.05	0.62	158
	4	14.1	0.13	0.23	0.04	0.04	99.8	0.003	0.132	0.0034	0.11	0.69	162
	Total	107.9											
Weighted averages			0.086	0.074	0.035	0.082	—	0.0036	0.086	0.0023	0.058	0.427	135
403. Magnesium in form of commercial billets, one-fourth added and melted before starting reduction, rest added during run.	1	30.8	0.13	0.06	0.03	0.13	99.75	0.002	0.051	0.0016	0.09	0.49	125
	2	28.6	0.12	0.14	0.03	0.11	99.2	0.002	0.062	0.0015	0.10	0.57	129
	3	27.2	0.16	0.07	0.04	0.08	99.75	0.002	0.055	0.0022	0.12	0.53	123
	4	17.2	0.19	0.25	0.03	0.02	99.5	0.002	0.074	0.0018	0.22	0.79	135
	Total	103.8											
Weighted averages			0.145	0.116	0.033	0.093	—	0.002	0.059	0.0018	0.122	0.572	127
404. Magnesium melted, settled, and siphoned before use to remove some of suspended impurities	1	29.5	0.04	0.08	0.03	0.04	99.9	0.002	0.039	0.0006	0.08	0.31	98
	2	26.3	0.06	0.17	0.04	0.06	99.4	0.003	0.052	0.0008	0.09	0.48	117
	3	26.3	0.13	0.04	0.03	0.09	99.6	0.003	0.058	0.0017	0.07	0.42	127
	4	24.0	0.15	0.12	0.03	0.11	99.3	0.002	0.070	0.0014	0.13	0.61	153
	Total	106.1											
Weighted averages			0.092	0.100	0.032	0.073	—	0.0025	0.054	0.0011	0.091	0.445	122

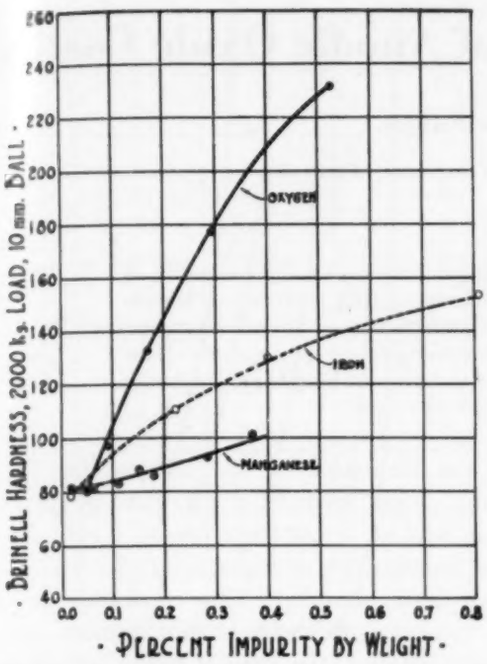

FIG. 8. Graph showing effect of oxygen, iron, and manganese on the hardness of titanium.

between amount of impurity and hardness of the as-melted ingot was determined. Electrolytic titanium[2] was used as the base, and the alloy additions were high grade commercial transformer iron, electrolytic manganese, and purified titanium dioxide. The alloys were made up by weight from the raw materials, but the actual composition of the melted ingot was determined by chemical analysis. Data obtained are shown in Fig. 8. The effects of all these elements as alloying additions to titanium have been studied before, but available data for iron and manganese did not indicate clearly the effect of such small amounts as are studied here. In the previous work on titanium-oxygen alloys (9–11), the oxygen content of the final alloy, on which hardness measurements were made, was not determined directly, and there was no assurance that the value taken was correct.

The curves show that the amount of manganese ordinarily present in commercial-grade sponge has little effect on the hardness, the iron content has more effect, and the oxygen most of all.

In the case of the various lots of sponge for which data are given in Table II, if separate increments of hardness due to manganese, iron, and oxygen by reference to Fig. 8 are estimated, it will be found that the sum is less than the amount the hardness of the batch exceeds that of pure titanium, about 60 BHN. This indicates, therefore, that the many other impurities present in very small amounts taken together also contribute significantly to the total hardness.

[2] Electrolytically purified in a small cell using a fused salt electrolyte. The purification was done in this laboratory.

ACKNOWLEDGMENTS

This project has been conducted at the Boulder City (Nevada) Experiment Station of the Bureau of Mines, now designated as the Electrometallurgical Branch of the Metallurgical Division, Region III, under the general supervision of R. R. Lloyd, Branch Chief. The authors are also grateful to C. T. Baroch for critical review of the manuscript, and to members of the Mechanical Services Section, under the direction of C. A. Stay, and of the Chemistry and Physics Section, under the direction of P. R. Perry, for valuable assistance in their respective fields.

Any discussion of this paper will appear in a Discussion Section to be published in the June 1955 JOURNAL.

REFERENCES

1. W. J. KROLL, *Trans. Electrochem. Soc.*, **78,** 35 (1940); U. S. Pat. 2,205,854, June 25, 1940.
2. R. S. DEAN, J. R. LONG, F. S. WARTMAN, AND E. L. ANDERSON, *Trans. Am. Inst. Mining Met. Engrs.*, **166,** 369 (1946).
3. F. S. WARTMAN, J. P. WALKER, H. C. FULLER, M. A. COOK, AND E. L. ANDERSON, *U. S. Bureau of Mines Rept. of Investigations* 4519, August 1949.
4. H. C. FULLER, D. H. BAKER, AND F. S. WARTMAN, *U. S. Bureau of Mines Rept. of Investigations* 4879, June 1952.
5. M. A. COOK AND F. S. WARTMAN, *U. S. Bureau of Mines Rept. of Investigations* 4837, February 1952.
6. C. K. STODDARD AND E. PEITZ, *U. S. Bureau of Mines Rept. of Investigations* 4153, December 1947.
7. None of the operations conducted by private companies, using the Kroll process, has been described in print. Aside from a few publications by various research organizations, one must rely largely on patents to gain some insight into the trend in this work. The following list is not complete and is intended only to give an idea of the various modifications proposed for the Kroll process:
   C. H. WINTER, JR. (assignor to E. I. du Pont de Nemours and Co.) U. S. Pat. 2,586,134, 2,607,674, 2,621,121.
   J. GLASSER AND C. HAMPEL (assignors by Mesne assignments to Kennecott Copper Corp.) U. S. Pat. 2,618,549 and 2,618,550.
   The British Aluminum Company, Ltd., and L. SAUNDERS, British Pat. 638,840.
   ROBERT D. BLUE (assignor to the Dow Chemical Co.) U. S. Pat. 2,567,838.
8. P. J. MADDOX AND L. W. EASTWOOD, *J. Metals*, **188,** 634 (1950).
9. R. I. JAFFEE, *ibid.*, **1,** 646 (1949).
10. R. I. JAFFEE, H. R. OGDEN, AND D. J. MAYKUTH, *ibid.*, **188,** 1261 (1950).
11. W. L. FINLAY AND JOHN A. SNYDER, *ibid.*, **188,** 277 (1950).

Factors Affecting the Formation of Anodic Oxide Coatings[1]

M. S. Hunter and P. Fowle

Aluminum Company of America, New Kensington, Pennsylvania

ABSTRACT

The effect of variations in electrolyte and forming conditions on the formation of porous type anodic oxide coatings on aluminum are discussed, with particular reference to the manner in which these variables control oxide formation, pore development, and the thickness of the barrier layer. Formation and solution rate data are applied to show that, during the formation of a porous type coating, conditions at pore bases are vastly different from those existing in the main body of the electrolyte.

Introduction

It has been known for many years that characteristics of the porous type of anodic oxide coating applied to aluminum are determined by the electrolyte used in its formation and by conditions under which it is formed. As a result, the structure of these coatings and factors that control their formation have been the subject of much discussion and investigation (1–7). Recently, structural features of the cells and pores comprising these coatings have been revealed, and methods have been developed for determining their dimensions (7, 8). The present paper establishes the effect of electrolyte and forming conditions on formation of the porous type of anodic oxide coating through the use of barrier layer thickness measurements (8), and presents a new concept of conditions that may exist at the bottom of the pores during the formation process.

When anodic oxide coatings are formed on aluminum, the chemical action of the electrolyte on the oxide governs the type of coating which results. If the electrolyte has no appreciable solvent action on the oxide, a thin nonporous barrier type of coating is formed. If, however, the electrolyte has appreciable solvent action, pores develop in the oxide, and the porous type of coating is produced. This latter type of coating is characterized by a thin nonporous barrier layer of oxide next to the metal and a relatively thick porous layer of oxide situated above the barrier layer. The entire coating is at one stage barrier layer oxide; the porous layer is barrier layer oxide, which contains tubular pores developed by solvent action of the electrolyte. The barrier layer at the bottom of the pores is important, because it constitutes an effective barrier between the metal and its environment during service.

[1] Manuscript received April 26, 1954. This paper was prepared for delivery before the Chicago Meeting, May 2 to 6, 1954.

In the formation of the porous type of oxide coating, oxide production proceeds in an orderly fashion and at a relatively constant rate, once the initial fluctuations which attend the start of this process have subsided. This constancy of barrier layer thickness indicates that a balance has been attained between the rate of oxide formation and factors controlling solvent action. Inasmuch as the thickness of the barrier layer is the net result of these competing actions, a change in this balance will be reflected in a change in thickness of the barrier layer. Consequently, changes in barrier layer thickness as a result of changes in electrolyte and forming conditions are an indication of the effect of these factors on formation of anodic oxide coatings.

Factors Affecting Barrier Layer Thickness

The balance between formation and solution of oxide is of a rather complex nature, because at least six major variables are involved: electrolyte type, electrolyte concentration, bath temperature, voltage, current density, and time. Electrolyte type, concentration, and temperature, along with current density and voltage, are interdependent, with the result that no variable may be changed without effecting a change in at least one other.

Considering the effect of the six major variables on barrier layer thickness, time is not a factor because it has been shown that barrier layer thickness remains constant with time, once the balance between formation and solution of oxide has been established (8). Further simplification may be made by considering first a single concentration of a specific electrolyte. An electrolyte containing 15% by weight of sulfuric acid was arbitrarily chosen as a starting point in this investigation.

With regard to the three remaining variables, voltage, current density, and bath temperature, it is found that they also are interdependent, and that

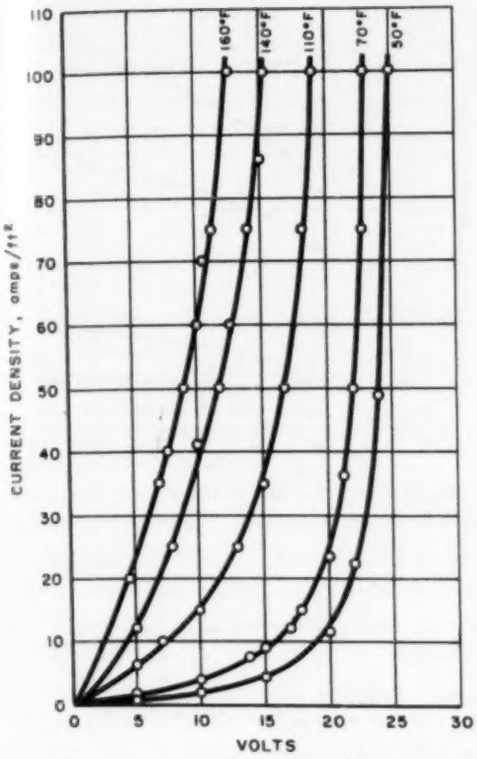

FIG. 1. Voltage, current density, and temperature relationships during coating of 99.99% aluminum in 15% sulfuric acid.

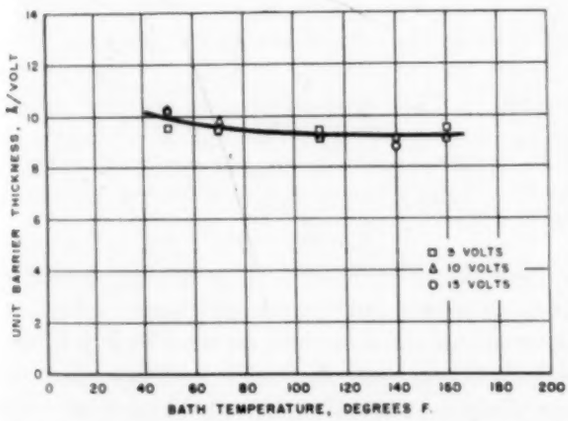

FIG. 2. Effect of voltage and temperature on unit barrier thickness for coatings on 99.99% aluminum formed in 15% sulfuric acid.

a change in one will be reflected in a change in one or both of the others (Fig. 1). Thus, if both temperature and forming voltage are chosen, current density is automatically established. Consequently, only the effects of forming voltage and bath temperature on barrier layer thickness need be considered initially.

The combined effect of these two variables on the unit barrier thickness (thickness per volt of forming potential) of coatings formed in the 15% sulfuric acid electrolyte is shown by Fig. 2. It is apparent that forming voltage in the range investigated had no effect on unit barrier thickness. Therefore, while forming voltage controls the total thickness of the barrier layer, it has no bearing on unit barrier thickness. Temperature, however, does have an effect on unit barrier thickness, and decreasing temperature results in greater unit barrier thickness. From the trend observed, it appears that at very low temperatures the unit barrier thickness will approach the 14 Å value characteristic of electrolytes that do not dissolve the oxide. This is not surprising, because solvent action of electrolytes generally decreases with temperature.

The effect of current density on unit barrier thickness may now be established by considering the interrelationship between this variable, forming voltage, and bath temperature. From Fig. 2, it is apparent that forming voltage did not affect unit barrier thickness. From Fig. 1, it is evident that for any given bath temperature the voltage range covered involved a wide range of current density values. Inasmuch as voltage had no effect on unit barrier thickness, it is apparent that current density also does not influence unit barrier thickness.

Having shown that voltage, current density, and time do not affect unit barrier thickness, it is possible to establish the effect of electrolyte concentration on unit barrier thickness by fixing bath temperature. For this part of the investigation, coatings formed at 15 volts in sulfuric acid electrolytes operated at 21°C were used. In the course of determining the relationship between barrier layer thickness and electrolyte concentration, it was observed that, at constant voltage, pronounced changes in current density occur with variations in sulfuric acid concentration (Fig. 3). The shape of the curve is similar to that of the curve for the conductivity of sulfuric acid solutions (9) (Fig. 3), although the highest current densities did not correspond to the maximum conductivities. Also, current densities were extremely low at both very low and very high acid concentrations.

Pronounced but not unexpected changes in unit barrier thickness were found to occur with variations in sulfuric acid concentration as shown by Fig. 4 and 5. As concentration was decreased to very low values (Fig. 4), the barrier approached the 14 Å/volt value characteristic of electrolytes that do not dissolve the oxide. This indicates that at very low concentrations the ability of the electrolyte to dissolve the oxide and develop pores decreases to an exceptionally low value. As concentration was increased in the range of 25–65% acid (Fig. 5), the unit barrier thickness did not vary appreciably, but at about 90% acid concentration and above, unit barrier thickness became practically zero. At these very high acid concentrations, no coating at

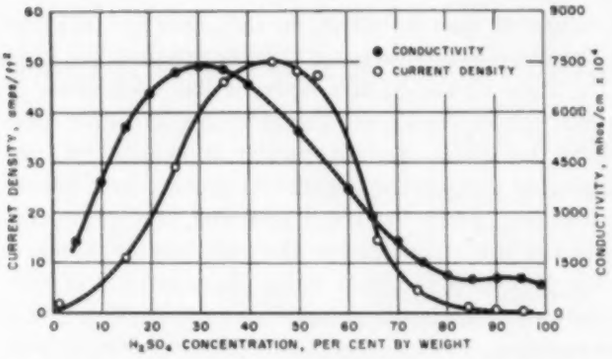

FIG. 3. Relation between concentration and conductivity of sulfuric acid solutions and between acid concentration and current density during coating of 99.99% aluminum at 15 v and 70°F.

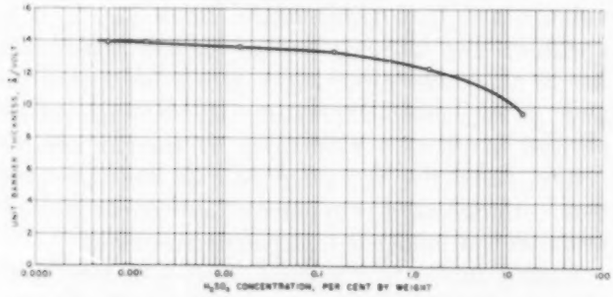

FIG. 4. Relation between concentration of dilute sulfuric acid electrolytes and unit barrier thickness of coatings formed on 99.99% aluminum at 70°F and 15 v.

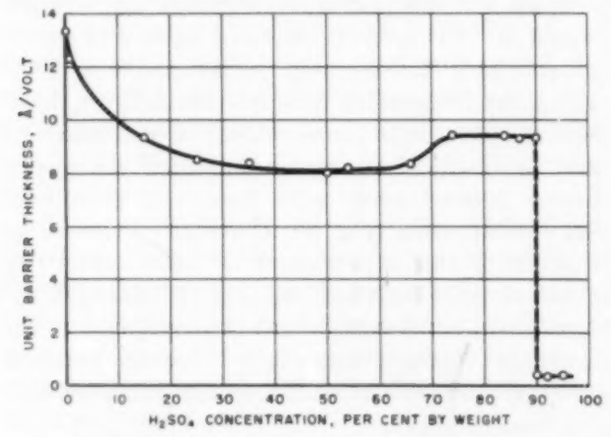

FIG. 5. Relation between sulfuric acid concentration and unit barrier thickness of coating formed on 99.99% aluminum at 70°F and 15 v.

all was formed, apparently because there was insufficient water present to ionize the electrolyte and form coating.

The effect of electrolyte type on unit barrier thickness was investigated by making barrier thickness determinations in 3% chromic acid, 4% phosphoric acid, and 2% oxalic acid electrolytes. In each of these electrolytes, unit barrier thickness changed appreciably with the bath temperature but did not change with variations in current density, voltage, and time, as was the case with the

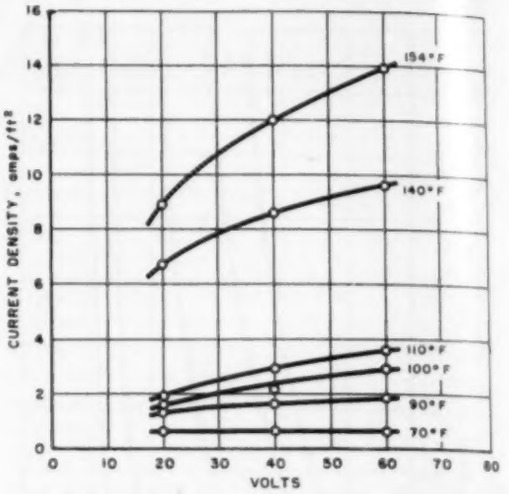

FIG. 6. Voltage, current density, and temperature relationships during coating of 99.99% aluminum in 3% chromic acid.

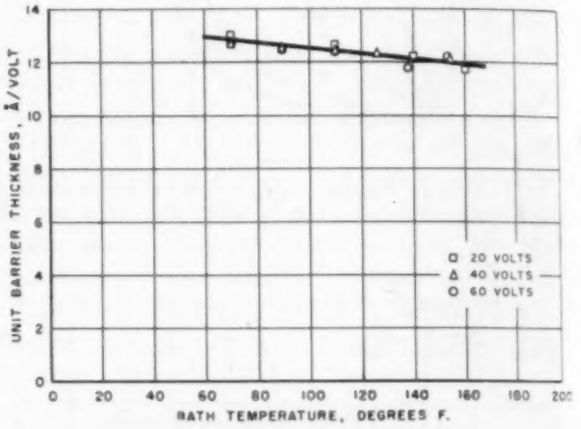

FIG. 7. Effect of voltage and temperature on unit barrier thickness for coatings on 99.99% aluminum formed in 3% chromic acid.

sulfuric acid electrolyte. Also, at any given temperature, different unit barrier thickness values were observed for the four electrolytes. The interrelationship between current density, voltage, and bath temperature, and the variation in unit barrier thickness with temperature for the 3% chromic acid electrolyte are shown by Fig. 6 and 7.

In summary, voltage, current density, and time control the amount of anodic oxide coating that forms, but these factors have no effect on unit barrier thickness. Unit barrier thickness is determined by electrolyte type, electrolyte concentration, and bath temperature.

FACTORS AFFECTING PORE FORMATION

Inasmuch as formation of the porous type of oxide coating involves a balance between oxide formation and solution, coating may form only as fast as solution occurs at the bases of the pores. In contrast to the formation of oxide which is an elec-

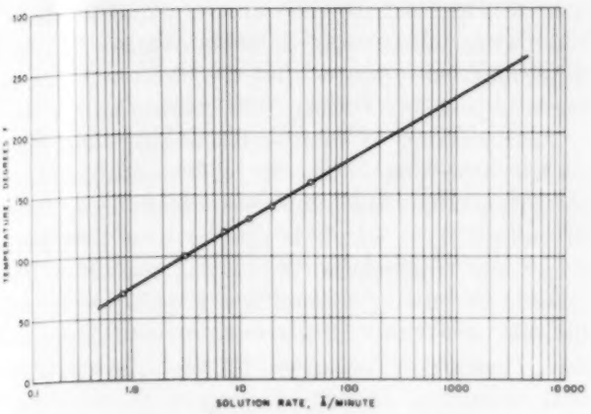

FIG. 8. Relation between solution rate and temperature in 15% sulfuric acid electrolytes.

trochemical process, solution of the oxide is primarily a chemical process. Of the six major variables under discussion, time may be eliminated by considering the rate of solution. Since the solution of oxide is a chemical process, current density will not have a direct effect but will affect solution rate only insofar as it may affect temperature. Voltage also will not affect solution rate directly but will influence the rate of solution insofar as it affects current density and temperature. Thus, the solution rate is defined in terms of electrolyte type, electrolyte concentration, and bath temperature, which are the same factors that control unit barrier thickness. In this investigation, only the effect of variations in concentration and temperature of sulfuric acid electrolytes has been investigated comprehensively, although preliminary work with other electrolytes has shown that electrolyte type has a pronounced effect on solution rate.

Solution rates were determined by immersing sulfuric acid anodic coatings in various concentrations of sulfuric acid at various temperatures without applied voltage. The reduction in thickness of the barrier layer resulting from immersion was then used to calculate linear solution rates in Angstrom units per minute.

Considering first the 15% sulfuric acid electrolyte that is used extensively in commercial applications, it is found that solution rate and temperature bear a logarithmic relationship (Fig. 8). Solution rate is doubled for every 8.6°C increase in temperature and is increased tenfold for every 28.3°C rise in temperature. These results are similar to those obtained by Hass (6) for the solution rates of barrier type oxide coatings in similar electrolytes. This relationship may be expressed more precisely by the equation

$$\log R = 0.0196T - 1.45$$

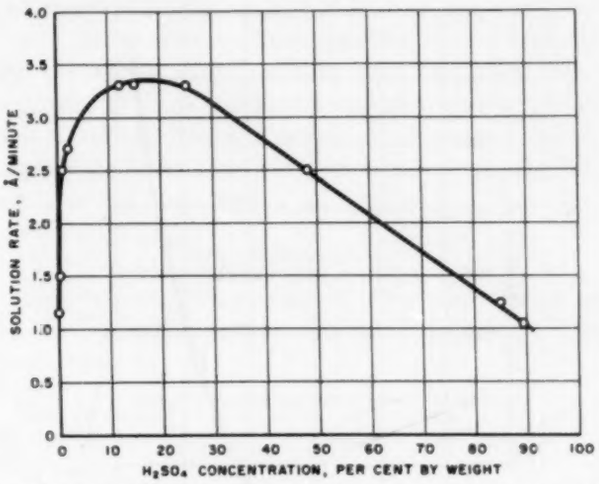

FIG. 9. Relation between solution rate and sulfuric acid concentration at 100°F.

where R is the linear rate of solution in Angstrom units per minute, and T is temperature in degrees Fahrenheit.

The specific effect of electrolyte concentration on solution rate was determined by measuring the decrease in thickness of the barrier layer portion of coatings formed in 15% electrolyte during exposure to electrolytes of other concentrations. At each concentration, the same logarithmic relationship was observed between temperature and solution rate. Thus, the plots of solution rate against temperature for various concentrations form a family of parallel lines on a semi-logarithmic plot. Solution rate varied somewhat with electrolyte concentration at all temperatures, but the effect of concentration was much less than that of temperature. Solution rate reached a peak in the range of about 12–25% acid. A typical curve showing the relation between concentration and solution rate is shown in Fig. 9. The sharp decrease in solution rate at very low concentrations is in keeping with the high unit barrier thicknesses observed at these concentrations.

From these relationships, it is apparent that temperature and electrolyte type and concentration control solution rate at the bases of the pores. Temperature is the dominant factor, and even relatively small changes in temperature result in pronounced changes in solution rate. Electrolyte concentration also affects solution rate, but rather large changes in concentration are required to produce significant changes.

Conditions Existing at Pore Bases

If formation rates and solution rates are considered further, an interesting hypothesis is evolved concerning the situation which may exist at the base of the pores during formation of the porous type of

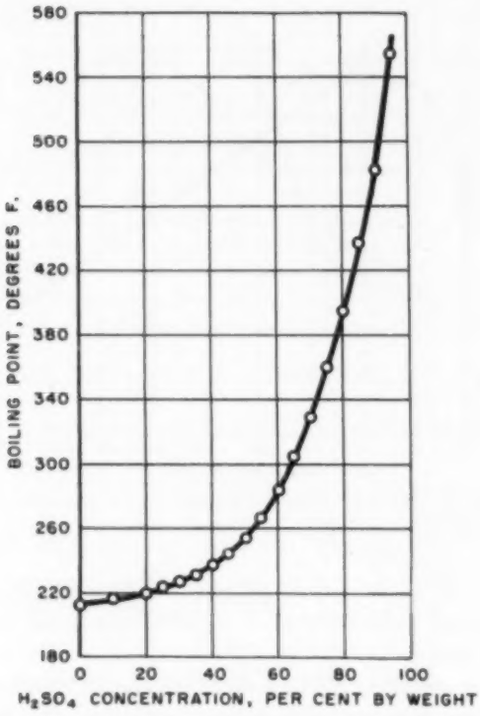

FIG. 10. Boiling points of sulfuric acid solutions

oxide coating. In the case of a coating formed in a 15% sulfuric acid electrolyte at 21°C using a current density of 12 amp/ft² (1.29 amp/dm²), oxide is formed at the rate of about 0.00088 in./hr, which amounts to 3725 Å/min. Inasmuch as the barrier thickness remains constant once the initial balance between formation and solution is established, the linear rate of solution at the base of the pores must also be 3725 Å/min. From data already presented, however, the linear rate of solution in 15% sulfuric acid at 21°C is only 0.84 Å/min. This difference in rate of over 4000:1 indicates that the electrolyte conditions at the base of the pores cannot be the same as those in the body of the electrolyte.

The conditions that probably exist at the base of the pores can be established from the solution rate data. From the solution rate formula given above, the 3725 Å/min rate which must exist to maintain constant barrier thickness corresponds to an electrolyte temperature of about 124°C for the 15% electrolyte. This is much higher than the boiling point of this electrolyte, and indicates that the electrolyte is probably of a concentration greater than 15%. Referring to the boiling points of sulfuric acid solutions (10) (Fig. 10), it is found that 124°C corresponds to the boiling point of 50% sulfuric acid. Thus, as a first approximation, the operating electrolyte at the base of the pores is boiling 50% sulfuric acid during the formation of this particular coating. Extension of this reasoning to cover the solution rate of the 50% acid instead of the 15% acid which could not develop the required solution rate brings about only a small change. The final determination indicates that the electrolyte at pore bases is probably boiling 51% sulfuric acid.

Consideration of other relationships that apply to the formation of anodic oxide coatings can be used to estimate the temperature and concentration of sulfuric acid which is operative at pore bases under any combination of forming conditions. The amount of coating formed is a function of current density and time in accordance with Faraday's law. The rate of formation, therefore, is a function only of current density. Consequently, other variables can affect the rate of formation only insofar as they affect current density. Also, rate of solution must equal rate of formation because the barrier thickness remains constant once the initial balance is established. Therefore, rate of solution also may be treated as a function of current density. Based on known rate of formation data, solution rate may be expressed by the equation:

$$R = 310\,C$$

where R is linear rate of solution in Angstrom units per minute, and C is current density in amperes per square foot.

As an example of the manner in which conditions existing at pore bases may be estimated, assume that a coating is to be applied in a 15% sulfuric acid electrolyte at 43°C using a potential of 10 volts. From Fig. 1, the current density corresponding to this voltage and temperature will be about 17 amp/ft² (1.83 amp/dm²). Rate of solution will be 310 times this value or about 4960 Å/min. From Fig. 8, a temperature of about 128°C is required to obtain this solution rate. This, in turn, corresponds to the boiling point of 53% sulfuric acid. Therefore, the electrolyte at pore bases under these conditions is approximately 53% acid at its boiling point of 128°C.

Further consideration of these various relationships reveals additional interesting information regarding the electrolyte operative at pore bases. The 15% sulfuric acid electrolyte has a solution rate of about 620 Å/min at its boiling point of about 103°C. This corresponds to a current density of about 2.0 amp/ft² (0.22 amp/dm²). At current densities below this value, the electrolyte at pore bases will be substantially 15% acid but will be at a temperature sufficient to give a solution rate corresponding to the particular current density value. At current densities above 2.0 amp/ft² (0.22 amp/dm²), the electrolyte will be at its boiling point and will be of a greater concentration and at a higher temperature to develop the solution rate required.

The existence of pronounced temperature and concentration differentials between the electrolyte at pore bases and in the body of the electrolyte emphasizes the importance of agitation in the anodic coating process. Movement of the electrolyte in and out of the pores is a very important factor in removing heat from the base of the pores where it is generated. Also, mixing of the electrolyte will tend to decrease the concentration gradient between the pore bases and the remainder of the electrolyte. Thus, agitation becomes a very important factor in the formation of the porous type of coating.

Conclusion

Consideration of the effects of the many variables which have been discussed emphasizes the fact that the formation of the porous type of oxide coating is a complex process and that, while formation is proceeding at a uniform rate, a delicate balance exists between formation and solution of oxide. Formation rate is primarily a function of current density and is affected by other factors only insofar as they may affect current density. Solution rate, on the other hand, is a chemical process and is determined by electrolyte type, concentration, and temperature. The barrier layer at the base of the pores, which is the net result of the balance between formation and solution, has a thickness which is apparently controlled by these same three variables—electrolyte type, electrolyte concentration, and bath temperature.

Application of the barrier layer measurement method to the anodic coating process shows that the conditions existing at the base of the pores are vastly different from those existing in the body of the electrolyte. Conditions at pore bases are characterized by high temperatures and high electrolyte concentrations, both of which are necessary to account for the relatively rapid rates at which these coatings can be formed.

Acknowledgment

The authors wish to express their appreciation to F. Keller under whose direction this work was conducted.

Any discussion of this paper will appear in a Discussion Section to be published in the June 1955 issue of the Journal.

REFERENCES

1. J. D. Edwards and F. Keller, *Trans. Electrochem. Soc.*, **79**, 135 (1941).
2. J. D. Edwards and F. Keller, *Trans. Am. Inst. Mining and Met. Engrs.*, **156**, 288 (1944).
3. I. Rummel, *Z. Phys.*, **99**, 518 (1936).
4. A. Jenny, "The Anodic Oxidation of Aluminum and Its Alloys," Charles Griffin and Company, Ltd., London (1940).
5. W. Bauman, *Z. Phys.*, **111**, 708 (1938).
6. G. Hass, *J. Opt. Soc. Amer.*, **39**, 532 (1949).
7. F. Keller, M. S. Hunter, and D. L. Robinson, *This Journal*, **100**, 411 (1953).
8. M. S. Hunter and P. Fowle, *ibid.*, **101**, 481 (1954).
9. "Handbook of Chemistry," N. A. Lange, Editor, 7th ed., p. 1412, Handbook Publishers, Inc., Sandusky, Ohio (1941).
10. "Chemical Engineers' Handbook," J. H. Perry, Editor, 2nd ed., p. 398, McGraw-Hill Book Co., Inc., New York (1941).

Polarographic and Coulometric Behavior of the Chloroacetaldehydes[1]

PHILIP J. ELVING AND C. EUGENE BENNETT

University of Michigan, Ann Arbor, Michigan

and

The Pennsylvania State University, State College, Pennsylvania

ABSTRACT

Chloral hydrate gives one apparently diffusion-controlled wave ($E_{1/2}$ about −1.4 v vs. S.C.E.), dichloroacetaldehyde two kinetic-controlled waves (−1.0 and −1.7 v), and chloroacetaldehyde two kinetic-controlled waves (−1.1 and −1.7 v). The chloral hydrate wave is actually controlled by a composite of diffusion and kinetic processes. Coulometric and polarographic data show that chloral hydrate is reduced to dichloroacetaldehyde hydrate; the latter dehydrates, and the unhydrated molecule is reduced to chloroacetaldehyde, which is then reduced to acetaldehyde; finally, the latter is reduced to ethyl alcohol or 2,3-dihydroxybutane, or both. This over-all reduction process forms only one wave; the acetaldehyde, whose reduction should result in a second wave, is formed in such a small amount that the wave is clearly demarcated in ammonia buffers only. Dichloroacetaldehyde is reduced to chloroacetaldehyde, which in turn is reduced to acetaldehyde with the formation of one wave; acetaldehyde reduction accounts for the second wave. Chloroacetaldehyde's first wave is due to reduction to acetaldehyde; the second due to reduction of acetaldehyde.

INTRODUCTION

Previous work on the electrochemical reduction of polyhalogenated compounds, particularly where more than one halogen is present on the same carbon atom, has indicated a general step-wise removal of halogen atoms (1–10). With a compound such as tribromoacetic acid, the first bromine comes off more readily than the second one, which in turn comes off more readily than the third. Of the three polarographic waves produced by tribromoacetic acid, the two more negative ones correspond to the two waves of dibromoacetic acid; the most negative wave corresponds to the one wave of bromoacetic acid.

In aqueous solutions, chloral hydrate gives one wave of $E_{1/2}$ about −1.4 v (an additional wave at −1.7 v is observed in ammonia buffers), and dichloroacetaldehyde and chloroacetaldehyde each give two waves at about −1.0 and −1.7 v, and −1.1 and −1.7 v, respectively. Since these results do not show the expected pattern, a complete study of the chloroacetaldehydes was made.

Reference to chloral hydrate is made throughout this paper since chloral exists as the hydrate in aqueous solutions. A few runs made with chloral (anhydrous before dissolution) gave polarograms similar to those of chloral hydrate.

EXPERIMENTAL

Stock aldehyde solutions (10 mM) were prepared from U.S.P. chloral hydrate,[2] a redistilled research sample of dichloroacetaldehyde,[3] a research sample of chloroacetaldehyde[4] [40.0% solution by weight; composition was checked by specific gravity measurement (11), sp gr 25/25°C 1.194], and acetaldehyde.[5] Nitrogen used for deoxygenating was purified and equilibrated by bubbling through sulfuric acid, an alkaline pyrogallol solution, water, and a portion of the test solution. Buffer solutions (Table I) were prepared from C.P. chemicals.

A Sargent Model XII Polarograph in connection with an external potentiometer and a Leeds and Northrup Type E Electro-Chemograph were used. A Beckman Model G *p*H Meter was used for *p*H measurement. All items of measuring apparatus were calibrated. A thermostated H-cell (12) employing a saturated calomel reference electrode was used. All potentials are referred to the saturated calomel electrode (S.C.E.) unless otherwise stated. The dropping mercury electrodes were prepared from Corning marine barometer tubing; the m and t values (open circuit, distilled water at 25°C, 60 cm head) for the capillaries used were: (*a*) 1.011 mg/sec and 5.0 sec (chloral hydrate); (*b*) 1.249 mg/sec and 4.6 sec (dichloroacetaldehyde); (*c*) 1.672 mg/sec and 4.0 sec (chloroacetaldehyde); and (*d*) 0.916 mg/sec and 5.6 sec (all three compounds). The coulometric runs using a stirred massive mercury cathode were made

[1] Manuscript received April 20, 1954.

[2] Merck and Company, 99.5% pure.

[3] Westvaco Chemical Division of the Food Machinery and Chemical Corporation, b.p. 87°C at 740 mm. n_D^{25} 1.4512.

[4] The Dow Chemical Company.

[5] Eastman Organic Chemicals.

TABLE I. *Buffer solutions*

Buffer	pH	Composition
1	1.4	0.5M KCl with added HCl
2	4.1–5.7	0.5M NaOAc with added HOAc
3	5.4	0.112M $Na_2HPO_4 \cdot 12H_2O$, 0.044*M* citric acid monohydrate, and 0.198*M* KCl
3	7.0	0.164M $Na_2HPO_4 \cdot 12H_2O$, 0.0176*M* citric acid monohydrate, and 0.073*M* KCl
4	8.3–9.6	0.5M NH_4Cl with added NH_3
5	9.2	0.082M $Na_2B_4O_7 \cdot 10H_2O$ and 0.32*M* KCl
5	9.8	0.082M $Na_2B_4O_7 \cdot 10H_2O$, 0.285*M* KCl, with added NaOH
6	10.5	0.163M $Na_2HPO_4 \cdot 12H_2O$ with added NaOH
6	12.3	0.105M $Na_2HPO_4 \cdot 12H_2O$ with added NaOH

in a modified Lingane (13) apparatus maintained at 25 ± 0.1°C.

The test solutions (ionic strength of 0.45 in all cases), prepared by mixing measured volumes of the stock and buffer solutions, had essentially the same *p*H as the buffer used. Five minutes was used for this operation. The test solution was deoxygenated for five minutes and then electrolyzed (ten minutes); the nitrogen atmosphere was maintained throughout the electrolysis.

Discussion

Using a fritted glass disk electrode, Neiman (7) reported the $E_{1/2}$ of chloral hydrate to be −0.8 v in 0.1*N* KCl (the reference electrode was not indicated); no interpretation of the wave was made.

After the present study was under way, Federlin (14) reported no reduction of dichloroacetaldehyde, one wave for chloral hydrate ($E_{1/2}$ of about −1.6 v) and two waves for chloroacetaldehyde (−1.1 and −1.8 v) with an additional wave appearing at −1.6 v at high *p*H values. He also found two waves for bromal (−1.3 and −1.8 v), two waves for dibromoacetaldehyde (−1.2 and −1.8 v), and two waves for bromoacetaldehyde (15) (−0.4 and −1.8 v), with an additional wave appearing at −1.6 v at high *p*H. The chloral wave was ascribed (14, 16) to a diffusion-controlled process involving reduction of the hydrated molecule to dichloroacetaldehyde, which was nonreducible; the first wave of chloroacetaldehyde was ascribed to a kinetic-controlled process involving reduction of the unhydrated molecule to acetaldehyde, and the second wave, to reduction of acetaldehyde. The additional wave which appeared only at high *p*H was ascribed to reduction of glycolic aldehyde (hydroxyacetaldehyde), the hydrolysis product of chloroacetaldehyde. Since reduction of dichloroacetaldehyde was not obtained, and since the explanation of the electrode process for chloral hydrate is inadequate, the work here reported was continued.

TABLE II. *Variation of current with drop time and temperature*

	Buffer No.	pH	Ratio of current at two heads of mercury[a, b]		Temperature coefficients[c]	
			Wave I	Wave II	Wave I	Wave II
Chloral hydrate	4	9.1	1.65		2.4	
	5	9.2	1.70		2.2	
Dichloroacetaldehyde	4	9.1	1.04	1.06	7.6	8.1
	5	9.8	1.0		8.1	
Chloroacetaldehyde	4	8.3	1.18	1.09	3.4	3.5
	4	8.9	1.24	1.12	3.6	3.7
	5	9.2	1.11		7.3	

[a] Corrected for back pressure by use of relation, $h_{back} = 3.1/m^{1/3}t^{1/3}$.

[b] With the following capillaries and the heads used, theoretical values for different current controlling processes are:

	Diffusion	Adsorption	Kinetic
(*a*) chloral hydrate	1.43	2.05	1.0
(*b*) dichloroacetaldehyde	1.23	1.51	1.0
(*d*) chloroacetaldehyde	1.23	1.51	1.0

[c] Calculated from the compound interest formula,

$$(\tau_2)^{i_1} = (\tau_1)^{i_1}\,(1 + \text{temp coeff.})^{(\tau_2 - \tau_1)}$$

The chloroacetaldehydes were found to possess a very complex electrochemical reduction pattern. For example, variations of current with drop-time, i.e., head of mercury, and temperature (Table II) indicate that a diffusion process may control the one chloral hydrate wave, while kinetic processes control both waves of dichloroacetaldehyde and of chloroacetaldehyde.

The Ilkovic equation, when applied to chloral hydrate data (Table III), indicates that about two electrons /molecule are consumed in the reduction process. Since an over-all two-electron transfer did not seem reasonable for chloral hydrate, and since the Ilkovic equation cannot be applied to kinetic-controlled processes, coulometric electrolyses were made on all three aldehydes to aid in establishing the electrode reactions.

In order to clarify the apparently unconnected behavior observed, the following discussion of polarographic and coulometric behavior of chloroacetaldehydes utilizes some of the conclusions subsequently summarized in the section on nature of the reduction process.

Polarographic Behavior

Polarographic data for the chloroacetaldehydes are given in Tables III, IV, and V. Apparent diffusion current constant values ($I = i_d/\mathrm{C}\, m^{2/3}\, t^{1/6}$) were calculated in the case of chloral hydrate to facilitate current comparison. Where the limiting current is not largely diffusion-controlled, it is designated as i_1.

TABLE III. *Effect of pH, concentration, drop time (head of mercury), and temperature on polarographic behavior of chloral hydrate*

Buffer[c] No.	pH	Conc. m*M*	Head cm	$-E_{1/2}$ v	i_d[a] μa	I[a]	α	n[a]
3[d]	7.2	0.25	40	1.42	0.86	2.60	0.35	1.4
4[d,f]	8.4	0.25	40	1.34	1.15	3.48	0.31	1.9
4[e,f]	8.9	1.0	60	1.32	4.23		0.34	
4[f]	9.1	1.0	40	1.32	3.60	3.64	0.32	1.9
4	9.1	1.0	80	1.36	5.94	4.98	0.32	2.6
4[e]	9.1	1.0	80	No wave detected				
4[b]	9.1	1.0	80	1.45	3.33	2.79	0.29	1.4
5	9.2	1.0	40	1.42	3.04	3.07	0.29	1.6
5	9.2	1.0	80	1.45	5.18	4.34	0.37	2.2
5[e]	9.2	1.0	80	No wave detected				
5[b]	9.2	1.0	80	1.51	3.00	2.51	0.29	1.3
5	9.8	1.0	40	1.65	2.56	2.59	0.25	1.3
5	9.8	1.0	80	1.67	3.84	3.22	0.32	1.7
5[b]	9.8	1.0	80	1.51	3.18	2.66	0.33	1.4
6	10.5	1.0	80	Wave too small to measure				
6	12.3	1.0	80	No wave detected				

[a] The i_d for chloral hydrate is pseudodiffusion-controlled and does not give true I and n values (see Discussion). The diffusion coefficient used was 1.0×10^{-5} cm² /sec [approximated from the value for trichloracetic acid (3) since the two compounds have similar molecular weights].

[b] Temperature was 0° C in these runs; it was 25° in all other runs.

[c] These runs were made 24 hr after mixing chloral hydrate and buffer.

[d] Capillary *c* was used for these runs.

[e] Capillary *d* was used for this run; capillary *a* was used in other runs.

[f] A second wave of $E_{1/2}$ about −1.66 v was observed in ammonia buffers (see Fig. 1 and Discussion).

Values of α were calculated from the slope of the wave by the relation, $\alpha = 0.056/(E_{1/4} - E_{3/4})$ at 25°. Typical polarograms of chloroacetaldehydes are shown in Fig. 1, the current vs. *p*H relationships in Fig. 2, and the $E_{1/2}$ vs. *p*H relationships in Fig. 3.

Chloral.—One cathodic wave ($E_{1/2}$ about −1.4 v) was obtained for chloral hydrate in the *p*H range of 7.0 to 9.1 with an additional wave appearing at −1.7 v in ammonia buffers (Fig. 1); a new wave due to reduction of chloroform (produced by the haloform reaction) appeared at −1.65 v in borate buffer at *p*H 9.8. The chloroform wave disappeared at higher *p*H as a result of its faster formation and subsequent disappearance during deoxygenating due to its volatilization and possible hydrolysis. No wave was detected in buffer 1 due to the prior hydrogen discharge wave. In buffer 2, a wave began, but the hydrogen wave appeared before its completion.

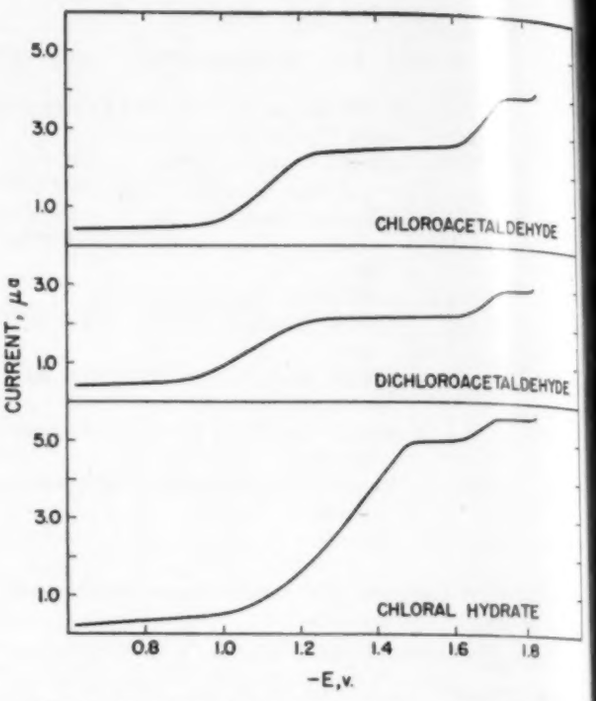

FIG. 1. Tracings (average current) of polarograms of 1.00m*M* solutions of chloral hydrate and chloroacetaldehyde, and a 0.99mM solution of dichloroacetaldehyde in ammonia buffer at *p*H 8.9 (60 cm mercury head, 25°C, capillary *d*).

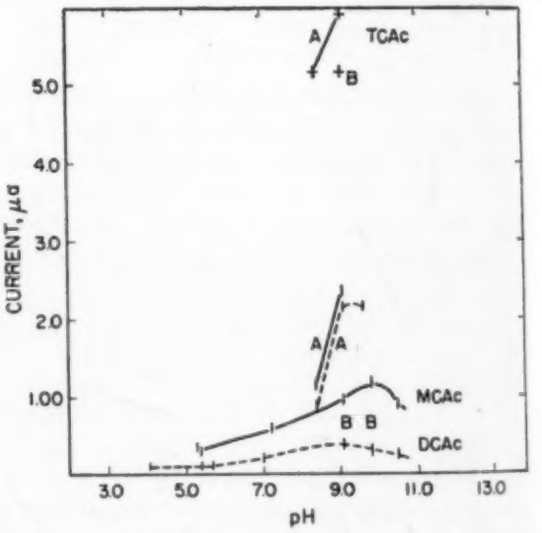

FIG. 2. Variation of the reduction current of the chloroacetaldehydes with *p*H. TCAc indicates chloral hydrate; DCAc and dashed lines indicate wave I of dichloroacetaldehyde; and MCAc indicates wave I of chloroacetaldehyde. *A* represents data in ammonia buffers and *B* in borate buffers. Magnitude of the currents can be compared only qualitatively since different capillaries were used.

Data are insufficient for any valid conclusions concerning the effect of *p*H on $E_{1/2}$. The current at *p*H 9.1 is greater in ammonia buffer than in borate; this is probably due, as will be shown later, to the greater currents of dichloro- and chloroacetaldehyde in

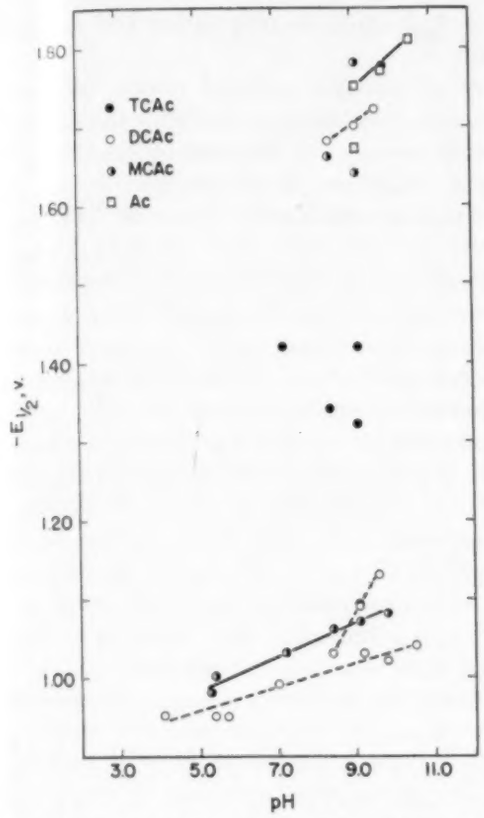

FIG. 3. Variation of $E_{1/2}$ with *p*H for chloral hydrate (TCAc), dichloroacetaldehyde (DCAc), chloroacetaldehyde (MCAc), and acetaldehyde (Ac). The precision of the $E_{1/2}$ values is about ± 0.02 v.

ammonia buffer which add to the over-all chloral hydrate wave.

Dichloroacetaldehyde.—In ammonia buffer two dichloroacetaldehyde waves ($E_{1/2}$ about −1.1 and −1.7 v) were obtained; the shift of the second wave to −1.54 in phosphate buffer (*p*H 10.4) is probably due to the reduction of glycolic aldehyde and glyoxal. Glycolic aldehyde may be formed at the electrode by hydrolysis of chloroacetaldehyde produced by dichloroacetaldehyde reduction, while glyoxal is formed by complete hydrolysis of dichloroacetaldehyde itself. The one wave at *p*H 12.3 evidently results from reduction of glyoxal (17). Only the first wave of dichloroacetaldehyde is observed in buffers 2 and 3 as the second wave is masked by buffer discharge.

$E_{1/2}$ for the first dichloroacetaldehyde wave increases slightly with *p*H except in ammonia buffers where a decided shift occurs (Fig. 3). The latter is due not only to *p*H change, but also to the increased formation of chloroacetaldehyde whose reduction still further enlarges the wave. Since $E_{1/2}$ of chloroacetaldehyde is slightly more negative than that of the dichloroacetaldehyde, such increase causes the midpoint of the composite wave to shift to a more negative potential.

Chloroacetaldehyde.—Two chloroacetaldehyde waves were obtained at about −1.1 and −1.7 v in buffers 4 and 5; an additional wave appeared at −1.55 v at *p*H values of 9.8 and greater. At *p*H 12.3, only the latter wave is observed; this wave is ascribed to reduction of glycolic aldehyde (14), the hydrolysis product of chloroacetaldehyde.

Acetaldehyde.—A few acetaldehyde runs were made in order to determine its $E_{1/2}$ in various buffer solutions. $E_{1/2}$ values found were −1.67 v in ammonia buffer at *p*H 9.1, −1.75 v in borate at *p*H 9.1, −1.77 v in borate at *p*H 9.8, and −1.81 v in phosphate at *p*H 10.5. An imine wave (18, 19) was observed at −1.35 v in ammonia buffer at *p*H 9.1.

Coulometric Behavior

Results of simple coulometric reduction of chloroacetaldehydes cannot be used as entirely conclusive evidence for the electrode process due to accompanying chemical processes; the data and their limitations will be discussed. Conclusive evidence for the nature of the electrode process was obtained by polarographically examining the solution at various stages in the coulometric reduction of chloral hydrate.

Behavior in ammonia solution.—In ammonia buffer, chloroacetaldehyde gave at −1.25 v and *p*H 8.4 values of 1.78 and 1.80 electrons per molecule, dichloroacetaldehyde (at −1.25 v) 3.14 (*p*H 8.4) and 3.16 (*p*H 9.1), and chloral hydrate (at −1.40 v and *p*H 8.4) 5.45 and 5.63 electrons per molecule. Results are difficult to interpret since carbonyl compounds generally react with ammonia to form reducible imines (18, 19); high, low, or "true" values could be obtained if such compounds were formed, e.g., (*A*) if the products obtained from carbon-halogen bond fission would form reducible imines, high values would be obtained; (*B*) if imines were formed from the original chloroacetaldehydes, in which both entities (carbon-chlorine bond and imine group) were nonreducible, low results would be obtained; (*C*) if the imine bond were reducible while the carbon-chlorine bonds were nonreducible in the imines formed from the original chloroacetaldehydes, low results would be obtained with chloral hydrate and dichloroacetaldehyde (polyhalogens, one imine group per molecule) while correct values would be obtained with chloroacetaldehyde.

The applied potential in chloral hydrate reduction is sufficient to reduce the imine of acetaldehyde if it were produced. The current of the first wave of dichloro- and chloroacetaldehyde is considerably higher in ammonia than other buffers; thus, imine reduction may be occuring at the potential needed for carbon-halogen bond fisson.

The three chloroacetaldehydes chemically decompose to form products which are reduced only at more

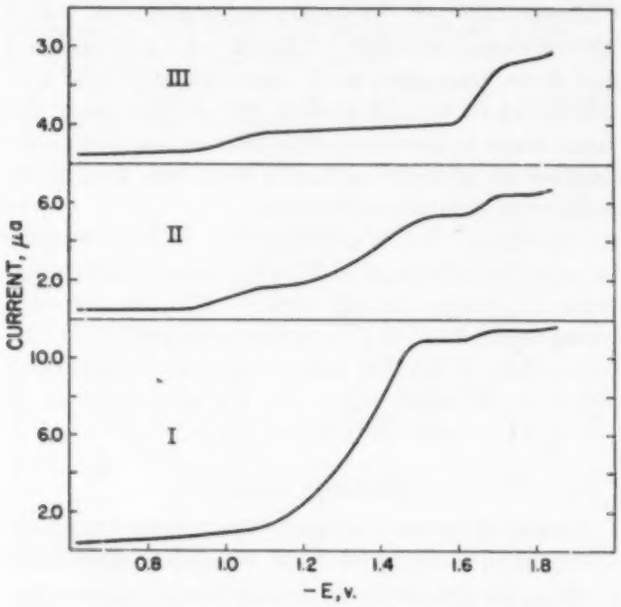

FIG. 4. Tracings of polarograms showing various stages in the coulometric reduction at −1.4 v of chloral hydrate in ammonia buffer of *p*H 8.4: I, before reduction; II, after a short period of reduction; III, after additional reduction.

negative values than the applied potentials used; this factor would tend to make observed coulometric values lower than true value. Decomposition is a major problem since electrolyses of these compounds generally require 10–15 hr/run because of the kinetic-controlled electrode processes; a diffusion-controlled process usually requires 1–2 hr for a two-electron reduction.

Behavior in borate and phosphate solutions.—In borate buffer (*p*H 9.2, −1.55 v), the value of 2.5 electrons obtained for chloral hydrate is low since, upon standing for the same length of time with no electrolysis, the concentration of chloral hydrate decreased to about one-third of the original amount. Kinetics of the processes involved are so complicated that no approximation of the true number of electrons transferred could be made by calculating the concentration actually reduced from the rate constants of the chemical and electrochemical reactions. Dichloro- and chloroacetaldehyde runs were not made in borate buffer due to the problem of chemical decomposition.

In McIlvaine buffer (*p*H 8.0, −1.50 v), chloral hydrate gives a value of about two electrons which is probably low due to observed chemical decomposition and to a possible interaction between chloral hydrate and the phosphate species present. Chloroethanol undergoes such a reaction (20), as apparently does trichloroethanol (21); due to its *gem*-diol structure, chloral hydrate may behave similarly.

Runs on chloroacetaldehyde (−1.20 v, McIlvaine buffer, *p*H 8.0) gave 1.1 and 1.2 electrons per molecule; these values are probably low due to similar observed chemical decomposition and reaction with phosphate.

Nature of partially reduced chloral solutions.—As mentioned, conclusive evidence for the nature of the electrode process was obtained by examining chloral hydrate solutions polarographically at various stages in their coulometric reduction. The same type of behavior was observed in all three buffers used (McIlvaine, ammonia, and borate). Results obtained in ammonia buffer are illustrated in Fig. 4; waves are clearly delineated and can be compared to those of chloroacetaldehydes in ammonia buffer (Fig. 1). Before reduction began, one large wave at −1.35 v and a small wave at −1.65 v was observed; after a short period of reduction, an additional wave appeared at −1.04 v (corresponds to $E_{1/2}$ of dichloro- and chloroacetaldehyde) and the −1.65 v wave (corresponds to $E_{1/2}$ of acetaldehyde) increased in size; after additional reduction only the waves at −1.04 and −1.65 v remained. The wave at −1.65 v decreased upon standing and stirring.

It should be noted that chloroform, which may be produced by the haloform reaction, shows polarographic behavior similar to that of acetaldehyde. However, the height of this wave during and after a coulometric electrolysis is much higher than would be expected from any chloroform produced by the haloform reaction. Therefore, the major portion of the wave must be due to the electrochemical reduction product which is believed to be acetaldehyde.

Nature of the Reduction Process

Chloral.—The observed behavior of chloral hydrate is explicable by the reaction scheme shown in Fig. 5, which is based on chemical, polarographic, and coulometric characteristics of the compound. Observation of only one wave for chloral hydrate in buffers 3 and 5 is due to chloral existing only as the hydrate in aqueous solution. The latter is reduced to dichloroacetaldehyde hydrate which is in equilibrium with the unhydrated molecule. The unhydrated dichloroacetaldehyde is reduced to chloroacetaldehyde which is then further reduced to acetaldehyde; the latter, in turn, is reduced (22–24) to ethyl alcohol, 2,3-dihydroxybutane, or both. Since dichloroacetaldehyde and chloroacetaldehyde are reducible at about −1.1 v, which is more positive than $E_{1/2}$ for chloral hydrate, and since neither compound is present at the electrode until after reduction of chloral hydrate, the dichloro- and chloroacetaldehyde waves merge into the wave of chloral hydrate.

An acetaldehyde wave is not observed in chloral hydrate reduction in buffers 3 and 5, since formation and reduction of dichloro- and chloroacetaldehyde involve kinetic processes, and the concentration of

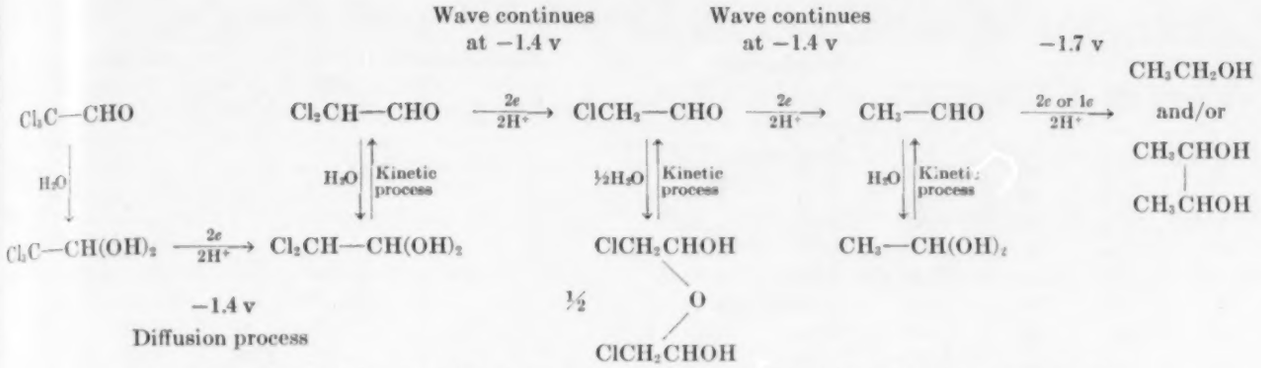

FIG. 5. Reaction scheme for the electroreduction of chloral hydrate and related compounds

TABLE IV. *Effect of pH, drop time (head of mercury), and temperature on polarographic behavior of dichloroacetaldehyde*[a]

Buffer No.	pH	Head cm	Wave I			Wave II		
			$-E_{1/2}$ v	i_l μa	α	$-E_{1/2}$ v	i_l μa	α
2	4.1	60	0.95	0.08	0.36			
2	5.4	60	0.95	0.09	0.38			
2	5.7	60	0.95	0.10	0.42			
3	7.0	60	0.99	0.16	0.37			
4	8.4	60	1.03	0.85	0.49	1.68	0.29	0.86
4[d]	8.9	60	1.08	1.58	0.46	1.68	0.55	1.1
4	9.1	60	1.09	2.18	0.42	1.70	0.49	1.1
4	9.1	90	1.10	2.33	0.41	1.70	0.51	1.1
4	9.1	60[b]	1.08	0.35		1.70	0.07	
4	9.6	60	1.13	2.15	0.46	1.72	0.68	1.1
5	9.2	60	1.03	0.39	0.33	[c]		
5	9.8	60	1.02	0.28	0.36	[c]		
5	9.8	80	1.03	0.28	0.40	[c]		
5	9.8	60[b]	1.03	0.04		[c]		
						Hydrolysis wave		
6	10.5	60	1.04	0.27	0.34	1.54	0.15	0.53
6	10.5	80	1.04	0.26	0.34	1.54	0.16	0.65
6	10.5	60[b]	1.03	0.05		1.54	0.03	0.65
6	12.3	60	No first wave			1.61	0.12	

[a] The concentration was 0.99 m*M* in all runs.

[b] The tempeature was 0° C in these runs; its was 25° in all other runs.

[c] Calculations were not made since the wave was poorly defined.

[d] Capillary *d* was used for this run; capillary *b* for all other runs.

acetaldehyde produced is insufficient to cause an observable wave. In ammonia buffer, larger amounts of dichloro- and chloroacetaldehyde are reduced (Tables IV and V) which in turn produce acetaldehyde in sufficient amount to cause an observable wave.

The Ilkovic equation indicates a two-electron process for reduction of chloral hydrate (see Table III) since the slow kinetic processes involved maintain the concentration of the reducible species formed at such a low level that their reduction adds little to the over-all wave height. Consequently, height and temperature coefficients (Table II) indicate a diffusion-controlled process, although the current is actually controlled by a combination of diffusion and kinetic processes.

Dichloro- and chloroacetaldehydes.—The reaction scheme of Fig. 5 also accounts for the observed behavior of dichloroacetaldehyde. The first wave is due to reduction to chloroacetaldehyde which, in turn, is reduced to acetaldehyde at a close enough potential so that only one wave is observed. The second wave corresponds to acetaldehyde reduction. Likewise, the first wave of chloroacetaldehyde is attributed to carbon-chlorine fission and the second wave to aldehyde reduction.

Dichloroacetaldehyde is more strongly hydrated than chloroacetaldehyde as indicated by the smaller current produced by its first wave; under diffusion-controlled conditions, the first wave of dichloroacetaldehyde (two carbon-halogen bonds are reduced) would be approximately twice the height of the first wave of chloroacetaldehyde. Since $E_{1/2}$ of dichloroacetaldehyde is much closer to $E_{1/2}$ of chloroacetaldehyde than expected, the dichloro species which is reduced in aqueous solutions is probably intermediate in structure between a hydrate and a free aldehyde.

Absence of the usually observed step-wise reduction pattern for carbon-chlorine bond fission in the chloroacetaldehydes accordingly results from the fact that different chlorinated species are being reduced. Actually, step-wise reduction does occur (Fig. 5) although only one halogen wave is observed for each of the three compounds.

Federlin's (14) failure to observe reduction of dichloroacetaldehyde may have been due to his experimental conditions. He used lithium chloride as the electrolyte, and ran in unbuffered medium and in buffered solution at *p*H 5.0 and 10.0. As shown in Fig. 2, the waves obtained for dichloroacetaldehyde at these *p*H values are quite small; therefore, at low instrument sensitivities, it is possible that a wave would not be observed.

Bromoacetaldehydes.—Federlin's interpretation of the

TABLE V. *Effect of pH, drop time (head of mercury), and temperature on polarographic behavior of chloroacetaldehyde*[a]

Buffer No.	pH	Head cm	Wave I			Hydrolysis wave			Wave II		
			$-E_{1/2}$ v	i_l μa	α	$-E_{1/2}$ v	i_l μa	α	$-E_{1/2}$ v	i_l μa	α
2	5.3	40	0.98	0.35	0.45						
2	5.3	60	0.99	0.42	0.45						
3	5.4	40	1.00	0.28	0.51						
3	5.4	60	1.01	0.29	0.48						
3	7.2	40	1.03	0.59	0.43						
3	7.2	70	1.01	0.66	0.48						
4[c]	8.3	60	1.06	0.89	0.46				1.64	0.55	1.1
4	8.3	90	1.06	1.05	0.45				1.65	0.60	0.94
4[b,c]	8.3	60	1.10	0.39	0.50				1.65	0.23	1.0
4	8.4	40	1.06	1.06	0.58				1.66	0.77	1.2
4[c]	8.9	60	1.11	1.89	0.53				1.68	1.35	1.1
4[c]	8.9	90	1.12	2.35	0.49				1.68	1.52	1.1
4[b,c]	8.9	60	1.15	0.79	0.49				1.69	0.55	1.2
4	9.1	40	1.09	2.33	0.56				1.64	1.69	1.2
5	9.2	40	1.07	0.95	0.49				1.78	0.67	0.71
5[c]	9.2	60	1.07	0.81	0.52				1.76	0.36	0.83
5[c]	9.2	90	1.08	0.90	0.49				1.77	0.43	0.78
5[b,c]	9.2	60	1.05	0.14	0.40				1.74	0.10	0.68
5	9.8	40	1.08	1.17	0.52	1.55	0.10		1.77	0.77	0.63
6	10.5	40	1.13	0.91	0.37	1.59	1.26	0.96			
6	12.3	40				1.64	1.09	1.1			

[a] The concentration was 1.0 mM in all runs.
[b] Temperature was 0°C in these runs; it was 25° in all other runs.
[c] Capillary *d* was used for these runs; capillary *c* for all other runs.

reduction mechanism of bromoacetaldehydes consists of the statement that the first wave is due to halogen reduction and the second wave to aldehyde reduction. This statement, although probably correct, does not account for the fact that only one halogen wave is obtained for each of the three compounds and does not explain the species involved in carbonyl reduction. He reported diffusion-controlled reductions of bromal and dibromoacetaldehyde which he attributed to reduction of the hydrated molecules. On the basis of the Ilkovic equation, he calculated the first wave in each compound to be a two-electron reduction process.

By reference to the present study of chloroacetaldehydes, reduction of the bromo analogs can be explained using Federlin and coworkers' data (14–16). Apparently, dibromoacetaldehyde hydrate is reduced to bromoacetaldehyde hydrate; the latter then dehydrates, and the unhydrated bromoacetaldehyde is reduced to acetaldehyde at approximately the same potential so that only one wave is observed. The second wave corresponds to acetaldehyde reduction. Insufficient data were reported for bromal hydrate to envisage precisely the reduction process; probably, however, bromal hydrate is reduced to dibromoacetaldehyde hydrate which is then reduced to bromoacetaldehyde hydrate; the latter dehydrates, and the unhydrated bromoacetaldehyde is reduced to acetaldehyde which subsequently is reduced to ethyl alcohol, 2,3-dihydroxybutane, or both.

Acknowledgment

The authors wish to thank the Atomic Energy Commission which helped support the work described.

Any discussion of this paper will appear in a Discussion Section to be published in the June 1955 issue of the JOURNAL.

REFERENCES

1. P. J. Elving, *Record Chem. Progr.* (*Kresge-Hooker Sci. Lib.*), **14,** 99 (1953).
2. P. J. Elving and C. L. Hilton, *J. Am. Chem. Soc.*, **74,** 3368 (1952).
3. P. J. Elving and C.-S. Tang, *ibid.*, **72,** 3244 (1950).
4. P. J. Elving and C.-S. Tang, *ibid.*, **74,** 6109 (1952).
5. P. J. Elving, I. Rosenthal, and M. K. Kramer, *ibid.*, **73,** 1717 (1951).
6. I. M. Kolthoff, T. S. Lee, D. Stovesova, and E. P. Parry, *Anal. Chem.*, **22,** 521 (1950).
7. M. B. Neiman, A. V. Ryabov, and E. M. Sheyanova, *Doklady Akad. Nauk S. S. S. R.*, **68,** 1065 (1949).
8. M. v. Stackelberg, "Polarographische Arbeitsmethoden," p. 212, Walter de Gruyter, Berlin (1950).
9. M. v. Stackelberg and W. Stracke, *Z. Elektrochem.*, **53,** 118 (1949).
10. L. B. Westover, M. S. Thesis, The Pennsylvania State College, State College, Pa. (1952).
11. Anon., "Chloroacetaldehyde," p. 5, The Dow Chemical Co., Technical Service and Development, Midland, Mich.

12. J. C. Komyathy, F. Malloy, and P. J. Elving, *Anal. Chem.*, **24**, 431 (1952).
13. J. J. Lingane, *J. Am. Chem. Soc.*, **67**, 1916 (1945).
14. P. Federlin, *Compt. rend.*, **232**, 60 (1951).
15. A. Kirrmann and P. Federlin, *Compt. rend.*, **230**, 1066 (1950).
16. A. Kirrmann, E. Saito, and P. Federlin, *J. chim. phys.*, **49**, C154 (1952).
17. P. J. Elving and C. E. Bennett, *J. Am. Chem. Soc.*, **76**, 1412 (1954).
18. P. Zuman, *Sbornik Mezinárod. Polarog. Sjezdu Praze, 1st Congr.*, 1951, Pt. I, Proc. 711.
19. P. Zuman, *Nature*, **165**, 485 (1950).
20. R. H. A. Plimmer and W. J. N. Burch, *J. Chem. Soc.*, **1929**, 286.
21. P. J. Elving and C. E. Bennett, *J. Am. Chem. Soc.* to be published.
22. W. Dirscherl and H. U. Bergmeyer, *Chem. Ber.*, **82**, 291 (1949).
23. R. Bieber and G. Trumpler, *Helv. Chim. Acta*, **30**, 2000 (1947).
24. G. Semerano and B. Polacek, *Gazz. chim. ital.*, **68**, 292 (1938).

Evolution of Stibine at Antimony Cathodes[1]

H. W. Salzberg[2] and A. J. Andreatch

Naval Research Laboratory, Washington, D. C.

ABSTRACT

The formation of stibine at antimony cathodes was studied by absorbing the cathode gas and analyzing the solution for antimony. The parameters studied were *p*H, salt concentration, temperature, and current density.

Results indicated that stibine was formed by the electrochemical discharge of a water molecule upon an antimony atom which was in contact with either two adsorbed hydrogen atoms or an adsorbed hydrogen molecule. Rate of the reaction was found to depend upon the voltage difference between electrode and solution. The stibine formed was inert to acid, but was readily decomposed by alkali. Stibine is probably formed by discharge of a water molecule on two adsorbed hydrogen atoms or a hydrogen molecule. Decreased rates of stibine formation in highly acid solution are thought to mean that high voltages, and, therefore, high overvoltages are not associated with hydronium ion discharge, but with water discharge.

Introduction

This is a report of an experimental investigation into the evolution of stibine at antimony cathodes. It was undertaken in continuation of work already performed in these laboratories which has indicated that water is reduced at platinum (1) and lead (2) cathodes at current densities above 10–60 ma/cm^2, even in fairly strong acid. Previous reports on stibine formation were contradictory (3, 4) and were felt to be unreliable.

Experimental Technique

Method

This was in principle very simple. The mixture of cathode gases was swept out of the apparatus and into an absorption tube by means of a stream of finely divided hydrogen bubbles. The absorbing solution was then analyzed for antimony.

In practice there were several difficulties. Quantities of stibine were so small that a microanalysis had to be performed. The gas is so unstable that rapid flushing of the electrolytic cell was necessary, with care being taken, however, not to sweep the gas through the absorption tube. Also, *p*H changes around the cathode affected the observed rates. Finally, the reaction is voltage dependent and therefore sensitive to small amounts of impurities.

Apparatus

The cell was a large U-tube, equipped with a standard taper ground glass joint at each end, with a fritted glass gas inlet near the bottom of the cathode limb. This fritted glass inlet served to break the incoming stream of gas into small bubbles which would stir and scour the solution more effectively.

Ground glass fittings provided suitably gas-tight connections without the use of rubber or cement.

Electrodes were mounted in glass caps sealed to ground glass joints which fitted into the ends of the U-tube. Each cap had a gas outlet. The outlet on the cathode cap was a glass tube of 7 mm inner diameter which terminated in another ground glass joint.

The anode was a strip of bright platinum approximately 6 cm^2 in area connected to a platinum wire sealed into the cap. The cathode was an antimony cylinder mounted on the end of an iron shaft enclosed in a Teflon sleeve. The shaft was mounted in a glass rod sealed into the glass cap. The space between the wall of the glass and the Teflon was filled with polyethylene to prevent gas leaks. The space between the antimony cylinder and the Teflon sleeve was also covered with polyethylene to prevent contact between solution and iron shaft. The flat bottom of the cylinder was covered with polyethylene, leaving as the working surface of the cathode a ring of antimony between the two polyethylene surfaces. This, it was felt, would maintain an approximately uniform current density over the electrode surface.

The absorption tube was a glass bubbler with a ground glass tip on the inlet which fitted into the joint on the outlet of the cathode cap. The absorbing solution was about 40 cm from the cathode.

Current was obtained from the power line, regulated with a Variac-rectifier and measured with a precision ammeter. Time was measured with a stopwatch.

[1] Manuscript received May 18, 1953. This paper was prepared for delivery before the Chicago Meeting, May 2 to 6, 1954.

[2] Present address: 171 East 90th Street, New York, N. Y.

Materials

All solutions were made from C.P. analyzed emicals. The scouring gas was tank hydrogen ssed over hot copper to remove oxygen. The abbing solution used was 6% mercuric chloride in HCl.

The antimony used was C.P. analyzed grade, ntaining no more than 0.04% of arsenic and 005% of iron. The electrode was cast in glass d machined down to proper dimensions, which re, finally, 0.77 cm diameter and 1.27 cm in ight. After machining, the electrode was cleaned peatedly by etching with HCl, HNO_3, and hot sh aqua regia. This etching process was repeated equently during the course of these experiments d check runs were made before and after cleaning minimize the effect of impurities depositing out ring the runs.

Procedure

After introducing the electrodes and the solution to the cell, the solution was scoured with hydrogen r 5 min to remove as much dissolved oxygen as ssible. The absorption tube was then inserted d current was started. Amounts of stibine obined were linear with time and the time of current ssage was therefore varied from run to run so as obtain optimum amounts of absorbed stibine for alysis. All results have been calculated on a 5-min me interval basis.

After cutting off the current, the cell was flushed e more minutes before removing the absorption be. This removed all stibine from the gas space er the electrode and the electrolytic solution. The ell was also flushed for 2–3 min between runs to move any oxygen which might have diffused over om the anode limb.

No provision was made to flush out the anode ompartment. The small amount of oxygen which ould diffuse the 5 cm from the anode through the nstirred anolyte to the bend in the U-tube, in the hort time of the experiment, would be flushed apidly away by the hydrogen stream. Any small mount eventually reaching the surface of the athode should have little effect at these high urrent densities. In retrospect, this is a potential ource of error and, in future work, both limbs will e flushed or separated with a diaphragm.

The absorbing solution was about 97–98% efficient, as determined by inserting a second bubbler in series with the first. The flow rate was set at about 200 cc of gas/min and regulated with a flow meter and valve.

Analysis was made by the standard Rhodamine-B method, which is accurate and precise to less than a microgram. This precision is far greater than that of the over-all experimental results.

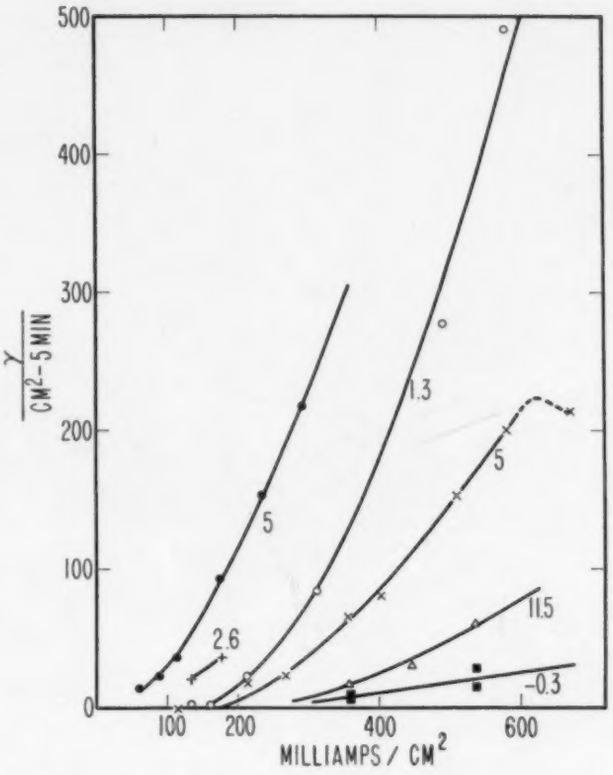

FIG. 1. *p*H effect, 25°C

	*p*H	Acid and alk.	Salt
■	−0.3	2–4*M* H_2SO_4	
○	1.3	H_2SO_4	0.4*M* Na_2SO_4
+	2.6	H_2SO_4	
×	5.0		1*M* Na_2SO_4
△	11.5	NaOH	
●	5.0		1*M* $(NH_4)_2SO_4$

Some solutions were used for individual runs, others for a whole series. There were frequent checks run, some after several months, to see if the results were reproducible from day to day and solution to solution.

Experimental Results

Results are shown in Fig. 1 to 4. These give the amounts of stibine detected as micrograms per square centimeter of cathode surface per 5-min interval, or as current passed, plotted against current density. These indicate the following:

1. Stibine evolution increases with current density at a greater than linear rate.

2. Maximum amounts of stibine detected were produced in neutral solutions buffered with ammonium ions (to minimize *p*H changes at the cathode). Buffered solutions show an increase in rate up to at least *p*H 5, while unbuffered solutions show a maximum at about *p*H 2.6 to 3.

3. Increasing acidity or alkalinity in the cell

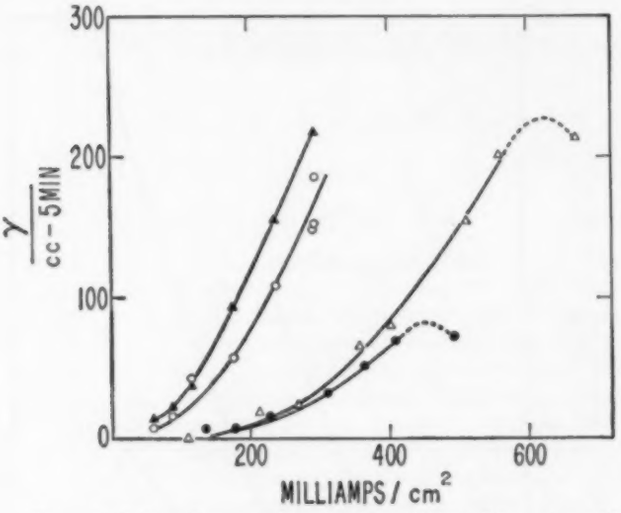

FIG. 2. Salt effect, 25°C. ▲—M $(NH_4)_2SO_4$; ○—$4M$ $(NH_4)_2SO_4$; △—M Na_2SO_4; ●—$\frac{1}{2}M$ Na_2SO_4.

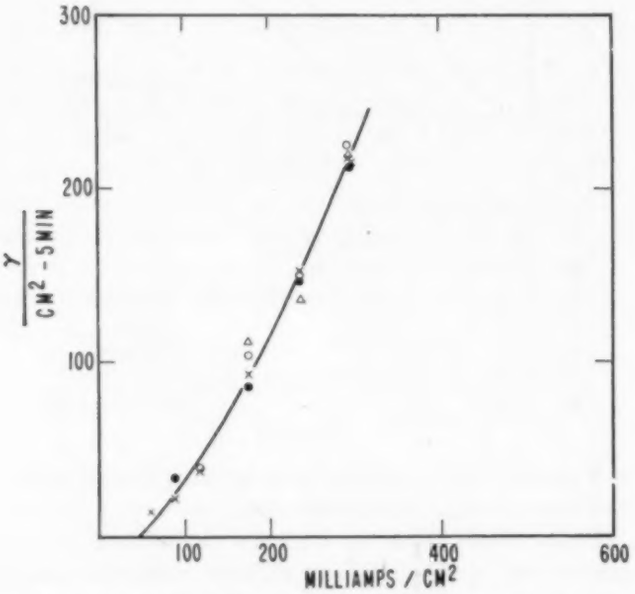

FIG. 3. Temperature effect, pH 5. ×—25°C, $1M$ $(NH_4)_2SO_4$; ○—5°C; ●—5°C; △—35°C.

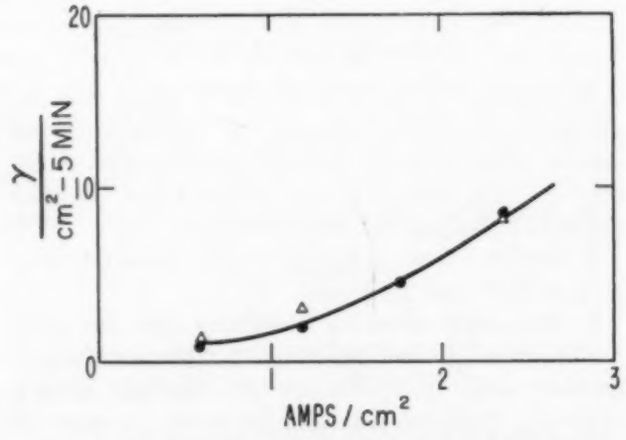

FIG. 4. Temperature effect, acid. △—5°C $2M$ H_2SO_4; ●—35°C $2M$ H_2SO_4.

lowers the amount of stibine absorbed in the bubbler, alkaline solutions showing lower amounts of stibine than acid solutions of the same concentration.

4. Higher salt concentrations in the cell gave smaller amounts of stibine in the bubbler, except for unbuffered solutions at high current densities. In this case, more concentrated solutions had lower rates than more dilute ones at low currents only and had higher rates at higher current densities. This crossover may be due to experimental error.

5. There is no appreciable temperature effect in the range from 5° to 35°C, in buffered neutral solutions and in acid solutions.

6. Amounts of stibine actually absorbed are very small, being at most about a milligram per square centimeter per five minutes of current passage.

7. At higher current densities in the unbuffered neutral solutions there is a decrease in the amounts of stibine absorbed.

Further qualitative observations which are not shown in the graphs are as follows:

8. Variations in rate of flow of the flush gas in neutral and acid solutions had no effect on the amounts of stibine absorbed in the receiver. No flow rate variations were run in alkaline solutions.

9. A black powdery antimony precipitate formed on the walls and in solutions with alkaline solutions, as reported by Sand and coworkers (3, 4), but not with acid solutions.

10. Traces of lead, added as the acetate, resulted in greatly increased stibine production.

11. Allowing metallic antimony to contact the surface of a mercury cathode which was evolving hydrogen at about 80 ma/cm² resulted in the formation of very large amounts of stibine.

12. In the absence of oxidizing agents, stibine was not absorbed when bubbled through solutions of N/10 acid, N/10 alkali, distilled water or neutral salt. Some was absorbed by 40% KOH.

Discussion of Results

In the following discussion, it is necessary to remember that the graphs do not show amounts of stibine actually produced, but only amounts of stibine absorbed in the receiver, this being the difference between rates of production and of decomposition.

In the case of acid and neutral solutions, however, decomposition apparently does not take place during the short time the stibine remains in the cell. This is indicated by points 8 and 9 above. If stibine were being decomposed in the cell, a slower gas flow would lower the amounts received in the bubbler and also result in some antimony powder being